Geoscience Frontiers xxx (2017) 1–15

HOSTED BY

ELSEVIER

Contents lists available at ScienceDirect

China University of Geosciences (Beijing)

Geoscience Frontiers

journal homepage: www.elsevier.com/locate/gsf

Burial and exhumation history of the Xigaze forearc basin, Yarlung suture zone, Tibet

Devon A. Orme

Department of Earth Sciences, Montana State University, 226 Traphagen Hall, P.O. Box 173480, Bozeman, MT 59717-3480, USA

ARTICLE INFO

Article history:
Received 2 May 2017
Received in revised form
2 October 2017
Accepted 9 November 2017
Available online xxx

Keywords:
Xigaze
Tibet
Forearc basin
Thermochronology
Yarlung

ABSTRACT

The Cretaceous–Eocene Xigaze forearc basin is a crucial data archive for understanding the tectonic history of the Asian continental margin prior to and following collision with India during the early Cenozoic Era. This study reports apatite and zircon (U–Th)/He thermochronologic data from fourteen samples from Albian-Ypresian Xigaze forearc strata to determine the degree and timing of heating (burial) and subsequent cooling (exhumation) of two localities along the Yarlung suture zone (YSZ) near the towns of Saga and Lazi. Thirty-seven individual zircon He ages range from 31.5 ± 0.8 Ma to 6.06 ± 0.18 Ma, with the majority of grains yielding ages between 30 Ma and 10 Ma. Twenty apatite He ages range from 12.7 ± 0.5 Ma to 3.9 ± 0.3 Ma, with the majority of grains yielding ages between 9 Ma and 4 Ma. These ages suggest that the Xigaze forearc basin was heated to 140–200 °C prior to cooling in Oligocene–Miocene time. Thermal modeling supports this interpretation and shows that the samples were buried to maximum temperatures of ~140–200 °C by 35–21 Ma, immediately followed by the onset of exhumation. The zircon He and apatite He dataset and thermal modeling results indicate rapid exhumation from ~21 Ma to 15 Ma, and at ~4 Ma. The 21–15 Ma thermochronometric signal appears to be regionally extensive, affecting all the lithotectonic units of the YSZ, and coincides with movement along the north-vergent Great Counter Thrust system. Thrusting, coupled with enhanced erosion possibly related to the paleo-Yarlung River, likely drove Early Miocene cooling of the Xigaze forearc basin. In contrast, the younger phase of rapid exhumation at ~4 Ma was likely driven by enhanced rock uplift in the footwall of north-striking rifts that cross-cut the YSZ.

1. Introduction

The Tibetan Plateau is the archetypal record of collisional tectonic processes on Earth (e.g., Dewey and Bird, 1970; Allègre et al., 1984; Burg and Chen, 1984; Garzanti et al., 1987; Yin and Harrison, 2000). Prior to the India-Asia collision in the early Cenozoic Era, the Asian margin was Andean-style, consisting of a magmatic arc, forearc basin, and accretionary wedge of ophiolitic and sedimentary matrix mélanges from north to south (Gansser, 1980; Girardeau et al., 1984; Schärer et al., 1984; Einsele et al., 1994). Following initiation of collision by 58–60 Ma (Garzanti et al., 1987; DeCelles et al., 2014; Orme et al., 2015; Hu et al., 2016), there is a gap of ~30 Myr between early formed structures related to suturing and development of the Tethyan Himalaya thrust belt and later out-of-sequence deformation and synorogenic sedimentation (Yin et al., 1999; Murphy and Yin, 2003). The lack of preserved geologic record during this interval challenges our understanding of how the collision zone evolved between the Paleocene and Oligocene–Miocene, limiting our ability to develop tectonic models of India-Asia collision.

The geologic boundary between continental crust of Indian and Asian affinity—the Indus-Yarlung suture zone (IYSZ)—extends for >2000 km across southern Tibet and northwestern India at an average elevation of ~5000 m. A significant component of the IYSZ is the Early Cretaceous to Early Eocene Xigaze forearc basin, a 4–5 km-thick sequence of marine and non-marine strata that extend laterally for 550 km across the Yarlung segment of the suture zone (YSZ) in south-central Tibet (Fig. 1; Einsele et al., 1994; Dürr, 1996; An et al., 2015; Orme et al., 2015). This basin developed along the southern margin of Asia—the Lhasa terrane—during northward subduction of Neo-Tethyan oceanic lithosphere (Einsele et al., 1994). Following collision with India in the Paleocene, the basin transitioned from predominantly marine to non-marine deposition until cessation of

E-mail address: devon.orme@montana.edu.
Peer-review under responsibility of China University of Geosciences (Beijing).

https://doi.org/10.1016/j.gsf.2017.11.011

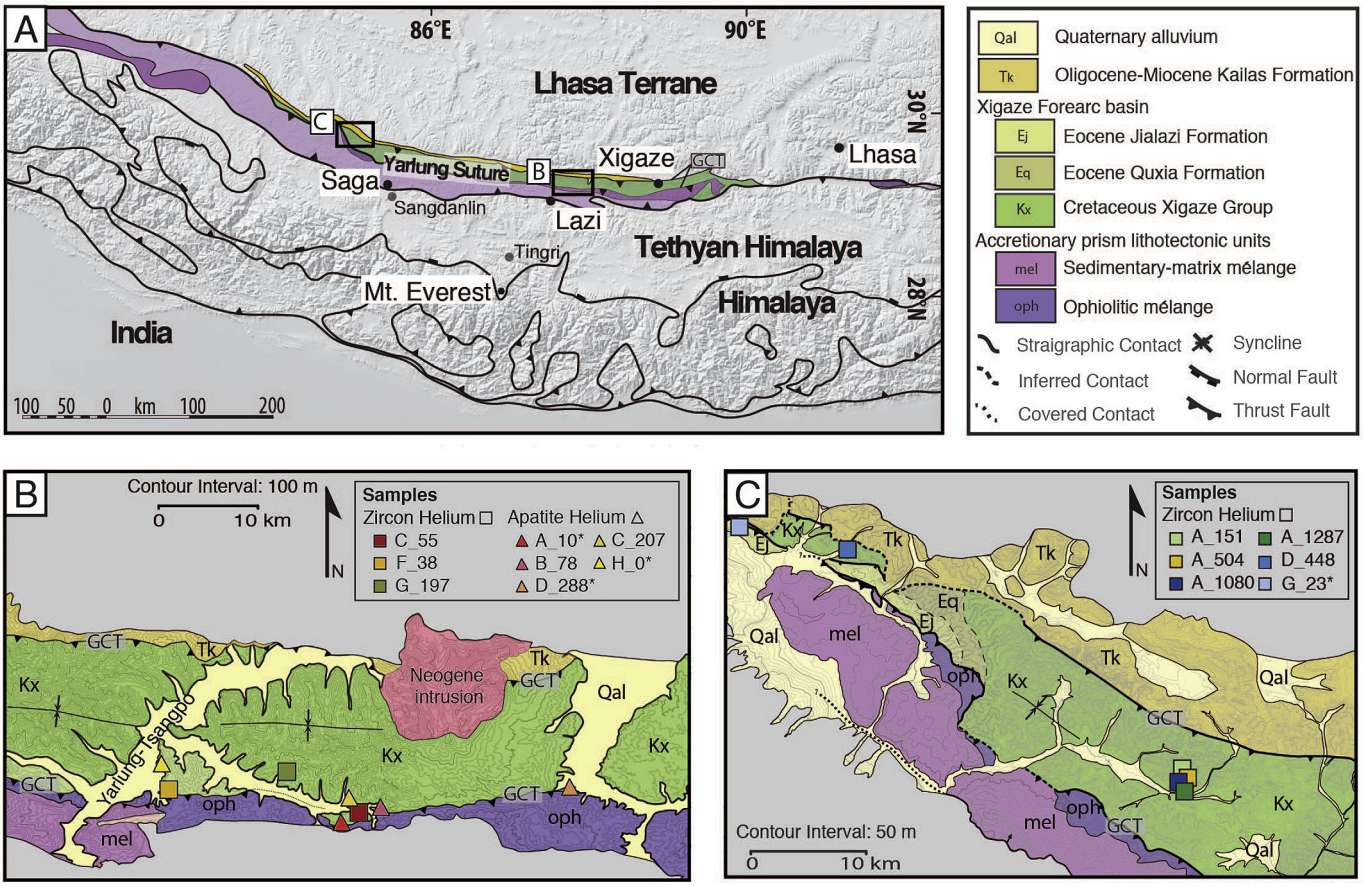

Figure 1. (A) Simplified geologic map of southern Tibet from Pan et al. (2004). Major elements of the Indus-Yarlung Suture Zone include, from north to south, the Oligocene–Miocene Kailas Formation, the Xigaze forearc basin, ophiolitic mélange, and sedimentary-matrix mélange. Digital elevation shaded relief base map from Global Multi-Resolution Topography Synthesis. (B) Geologic map of the Lazi study region from Orme and Laskowski (2016). (C) Geologic map of the Saga study region from Orme et al. (2015). Location of zircon and apatite (U–Th)/He samples shown by squares and triangles, respectively.

sedimentation ca. 51 Ma (Hu et al., 2015; Orme et al., 2015). Whether the Xigaze forearc basin was significantly buried by later sedimentation or thrust faulting, and the magnitude of this burial, is unknown. Alternatively, the Xigaze forearc basin might have been exhumed to modern exposure depths soon after the onset of collision. Geologic evidence for deformation and possible structural burial of the forearc basin is restricted to basin bounding north-vergent thrust faults, the Great Counter Thrust system (GCT) (Fig. 1). Displacement across the GCT occurred sometime between 25 Ma and 17 Ma (Heim and Gansser, 1939; Zhang et al., 2011; Laskowski et al., 2017), more than 26 Myr after deposition of the youngest Xigaze forearc basin strata. At present, the thermal history of the Xigaze forearc basin after ~51 Ma is unknown.

Low-temperature thermochronology is commonly applied to recover the thermal history of sedimentary basins (e.g., Sobel and Dumitru, 1997; Rhal et al., 2007; Fosdick et al., 2014). Specifically, apatite and zircon (U–Th)/He dating (apatite He and zircon He), which are based on the accumulation of ^{4}He produced by the alpha decay of the parent isotopes ^{238}U, ^{235}U, ^{232}Th, and ^{147}Sm, are often used to constrain thermal histories of rocks between 2 and 8 km in depth within Earth's crust (Zeitler et al., 1987; Farley, 2002; Reiners et al., 2004). Apatite He provides information on the timing and rates of cooling through ~40–80 °C (Farley, 2002), making it particularly sensitive to processes close to the Earth's surface. In contrast, zircon He constrains thermal processes between ~140 and 200 °C (Reiners et al., 2002, 2004; Guenthner et al., 2013). Zircon and apatite He dating can be combined with thermal modeling to extract the magnitude of heating (burial) and cooling (exhumation) of sedimentary basins, following cessation of deposition.

This study applies apatite and zircon (U–Th)/He thermochronology to sedimentary rocks from the Xigaze forearc basin to constrain its thermal history from Cretaceous to Pliocene time (~110–4 Ma). The aims of this study are to (1) constrain the maximum burial temperature and duration of heating prior to the India-Asia collision, (2) determine if the basin was buried further, and to what temperatures, following the onset of collision, and (3) determine the timing of basin exhumation. Results indicate that basin burial can be explained by sedimentation within the forearc region, possibly recording development of a suture zone successor basin, without the need for large magnitudes of structural burial. In addition, results support previous studies from the YSZ that document two stages of post-collisional exhumation at 20–15 Ma and 10–4 Ma. Thrusting across the GCT system, coupled with enhanced erosion, likely drove early Miocene exhumation. In contrast, late Miocene extension was likely driven by orogen-parallel (E–W) extension that produced N–S striking normal faults that crosscut the suture zone and exhumed forearc strata in their footwalls. These results fill a critical gap in our understanding of the evolution of the Himalayan-Tibetan orogenic belt.

2. Geologic setting

From north to south, the YSZ comprises the Kailas basin, Xigaze forearc basin, and accretionary prism lithotectonic units (Burg and Chen, 1984; Fig. 1). North of the Kailas basin, the Gangdese

Please cite this article in press as: Orme, D.A., Burial and exhumation history of the Xigaze forearc basin, Yarlung suture zone, Tibet, Geoscience Frontiers (2017), https://doi.org/10.1016/j.gsf.2017.11.011

magmatic arc primarily consists of Cretaceous–Paleocene and Eocene granitoid and volcanic rocks that were emplaced during subduction of Neo-Tethyan oceanic and Indian lithosphere, respectively (Allègre et al., 1984; Burg and Chen, 1984; Lee et al., 2009). Locally, Gangdese magmatic arc rocks are as young as late Miocene (Maluski et al., 1982; Schärer et al., 1984; Kapp et al., 2005). East of the field area, near the town of Zedong, the Gangdese Thrust juxtaposes Gangdese magmatic arc rocks over sedimentary rocks of the Indian passive margin (i.e., Tethyan-Himalaya; Yin et al., 1994). Timing of slip along the Gangdese Thrust is estimated to be 30–23 Ma based on $^{40}Ar/^{39}Ar$ thermochronology, which records cooling of hangingwall units during this time interval (Yin et al., 1994). South of the Xigaze forearc, the accretionary prism comprises ophiolitic and sedimentary matrix mélanges that define the southern extent of the suture zone (Fig. 1; Girardeau et al., 1984; Einsele et al., 1994; Cai et al., 2012; An et al., 2017; Metcalf and Kapp, 2017; Xiong et al., 2017).

The Xigaze forearc basin crops out along the YSZ as an east-trending syncline, ~20 km in width from north to south (Fig. 1). Its northern and southern boundaries are defined by north-vergent faults, mapped as part of the Great Counter Thrust system (GCT) (Heim and Gansser, 1939; Zhang et al., 2011; Laskowski et al., 2017). Along its southern margin, the forearc is primarily in the footwall of the southern thrust in the system (locally referred to as the Renbu-Zedong thrust; Yin et al., 1994), which places Aptian (~125–113 Ma) ophiolitic mélange atop forearc strata. Locally, the forearc is in depositional contact with the ophiolite (Huang et al., 2015; Orme and Laskowski, 2016). On its northern margin, forearc strata are thrust over Oligocene–Miocene conglomerate of the Kailas Formation, which were deposited as a buttress unconformity on Gangdese magmatic arc rocks between 26 and 18 Ma (DeCelles et al., 2011; Leary et al., 2016). The GCT system was active sometime between 25 Ma and 17 Ma based on crosscutting relationships, with possible timing variations along-strike (Quidelleur et al., 1997; Yin et al., 1999; Harrison et al., 2000; Carrapa et al., 2014; Leary et al., 2016; Laskowski et al., 2017). The dominant structural mode affecting the southern Tibetan Plateau and YSZ at present is orogen-parallel (E–W) extension, which initiated between 17 Ma and 14 Ma (e.g., Murphy and Copeland, 2005; Sundell et al., 2013; Styron et al., 2015). North-striking normal faults cut the YSZ and exhumed mylonitic shear zones in their footwalls (Kapp et al., 2008; Taylor and Yin, 2009; Laskowski et al., 2017).

The Xigaze forearc basin is divided into two stratigraphic groups: the Lower Cretaceous to Upper Cretaceous Xigaze Group (Einsele et al., 1994; Dürr, 1996; Wang et al., 2012, 2017; An et al., 2015; Orme and Laskowski, 2016) and the Upper Cretaceous to lower Eocene Tso-Jiangding Group (Ding et al., 2005; Hu et al., 2015; Orme et al., 2015). Provenance analyses indicate that forearc detritus was primarily derived from the Gangdese magmatic arc to the north (Einsele et al., 1994; Dürr, 1996; Wu et al., 2010; An et al., 2015; Orme et al., 2015; Hu et al., 2016). The stratigraphic units are oldest along the southern and northern margins of the basin and young towards the center of the syncline (Fig. 1B and C). The Xigaze Group is exposed along most of the central-segment of the IYSZ, but the Tso-Jiangding Group is only present northwest of the town of Saga (Fig. 1). Thus, it is necessary to study preserved stratigraphic intervals at multiple locations to capture the complete forearc stratigraphic record.

3. Previous thermochronologic data

Current constraints on the timing of exhumation of the IYSZ are primarily from thermochronologic data from the Gangdese magmatic arc, post-collisional Oligocene–Miocene Kailas basin, and modern river detritus. $^{40}Ar/^{39}Ar$, Apatite Fission Track (AFT), and apatite and zircon (U–Th)/He thermochronologic investigations of the Gangdese magmatic arc indicate accelerated cooling at ca. 52–42 Ma, ca. 26–17 Ma and ca. 15–10 Ma (Copeland et al., 1987; Harrison et al., 2000; He et al., 2007; Dai et al., 2013; Carrapa et al., 2014; Li et al., 2015; Tremblay et al., 2015; Carrapa et al., 2017). Zircon He ages from the Kailas Formation (~31–9 Ma) are partially reset and suggest basin burial to temperatures <230 °C (Carrapa et al., 2014). AFT and apatite He ages from the Kailas Formation indicate two episodes of rapid cooling at ca. 17 Ma and between 9 Ma and 4 Ma, respectively. Similarly, AFT ages from modern river detritus from the tributaries of the Yarlung River, which runs from west to east across the YSZ, document the same cooling signature during Miocene time (Carrapa et al., 2017).

Late Oligocene to Early Miocene cooling of the Gangdese magmatic arc is attributed to denudation during south-directed displacement along the Gangdese thrust, which is estimated to be active from 30 Ma to 23 Ma (Copeland et al., 1987; Yin et al., 1994; Harrison et al., 2000; Dai et al., 2013). Middle–Late Miocene cooling documented in both the Gangdese magmatic arc and Kailas Formation is interpreted to be driven by uplift-induced erosion coupled with efficient river incision by a paleo-Yarlung River (Cina et al., 2009; Carrapa et al., 2014, 2017) related to either capture by the Bramaputra in mid-Miocene time (Robinson et al., 2013; Bracciali et al., 2015), renewed underthrusting of India beneath Asia (DeCelles et al., 2011; Carrapa et al., 2017), and/or to intensification of the Asian monsoon in Late Miocene time (Quade et al., 1989; Sanyal et al., 2010).

Li et al. (2017) reported AFT and apatite and zircon (U–Th)/He dates from Albian-Santonian strata from a N–S transect of the Xigaze forearc, west of the town of Xigaze (Fig. 1). AFT central ages and single grain zircon (U–Th)/He ages are between 16.2 ± 3.2 Ma to 64.4 ± 2.6 Ma and 16.3 ± 1.0 Ma to 92.5 ± 5.7 Ma, respectively. These are interpreted to record burial by Xigaze foreland basin stratigraphy until ~34 Ma and to reflect a northward younging exhumation trend within the forearc related to Cretaceous–Miocene changes in India-Asia convergence (Li et al., 2017). In contrast, single grain apatite (U–Th)/He ages are Miocene, from 16.0 ± 1.0 Ma to 7.0 ± 0.4 Ma. Miocene cooling is interpreted as being related Great Counter Thrust shortening, which drove incision of the Yarlung River, resulting in exhumation (Li et al., 2017). However, movement along the GCT system ceased by ~16.5 Ma (e.g., Yin et al., 1999; Harrison et al., 2000; Carrapa et al., 2014; Leary et al., 2016; Laskowski et al., 2017), precluding it as a mechanism to explain cooling during Late Miocene time.

4. Methodology

4.1. Sample collection

This study focuses on two regions of the Xigaze forearc, which together expose 6.7 km of forearc stratigraphy deposited between 110 Ma and 51 Ma. The depositional ages used in this study come from fossil assemblages, U–Pb geochronologic crystallization ages from tuffaceous sandstone, and maximum depositional ages from U–Pb detrital geochronology reported in Orme et al. (2015) and Orme and Laskowski (2016). Within the first study area, northeast of the town of Lazi, ~2.7 km of stratigraphy deposited between 110 Ma and 85 Ma is preserved (Orme and Laskowski, 2016; Fig. 1B). In second study region, northwest of the town of Saga, ~4 km of strata deposited between 88 Ma and 51 Ma are preserved in the center of the syncline (Orme et al., 2015; Fig. 1C).

Fourteen medium- to coarse-grained sandstone samples, including four tuffaceous sandstone samples, were analyzed from the two studied regions of the Xigaze forearc. From these, eight sandstone samples and one tuffaceous sandstone sample were analyzed for zircon He and five samples yielded apatite suitable for

Please cite this article in press as: Orme, D.A., Burial and exhumation history of the Xigaze forearc basin, Yarlung suture zone, Tibet, Geoscience Frontiers (2017), https://doi.org/10.1016/j.gsf.2017.11.011

apatite He analysis. Within the Lazi area, eight samples deposited between 110 Ma and 93 Ma were analyzed for either apatite or zircon He (Fig. 1B). In the Saga area, six samples deposited between 90 Ma and 53 Ma were analyzed for zircon He (Fig. 1C). A gap in sampling exists between ~77 Ma and 55 Ma, where deposition within the basin was primarily shallow marine carbonates, resulting in a scarcity of clastic material (Ding et al., 2005; Orme et al., 2015). In addition, there is a well-documented magmatic lull in Gangdese magmatic arc activity from 75 Ma to 69 Ma, which may contribute to a lack of apatite and zircon derived from volcanic events within the basin (Lee et al., 2009). No samples have both apatite and zircon He ages as apatites suitable for He dating were rare or unavailable in the majority of samples.

4.2. Apatite and zircon (U–Th)/He dating

The Xigaze forearc basin preserves stratigraphic thicknesses >6 km, suggesting that the basin may have experienced temperatures >120–150 °C (assuming a geothermal gradient of 20–25 °C/km; e.g., Dumitru, 1991); therefore, the zircon He system may be sensitive to thermal processes active after deposition. In this study, zircon He is used to determine the maximum burial temperature and timing of initial basin cooling and exhumation. In turn, apatite He is used to determine the timing at which the basin cooled to within a few kilometers of Earth's surface.

Grain selection, He extraction and measurement, and isotopic dissolution for U-Th-Sm content were conducted at the University of Arizona Radiogenic Helium Dating Laboratory (ARHDL), following the methods described in Reiners et al. (2004). Three to six grains per sample were selected based on morphology, size, and grain clarity. Only euhedral grains of similar size from a sample with half widths >60 μm were selected. Thirty-seven zircon and twenty apatite grains were analyzed. Following grain selection and measurement (Farley, 2002; Hourigan et al., 2005), selected grains were placed in a 1 mm Nb foil envelope to avoid volatilization of parent nuclides during He extraction. A Nd:YAG laser, cryogenic purification and quadrapole mass spectrometer were used for He extraction analysis. Following He measurements, the Nb foil packets were transferred to Teflon vials for isotope dilution. All aliquots were spiked with a mixed spiked containing nominally pure ^{233}U and ^{229}Th, and, if apatite, a 98% pure ^{147}Sm spike. Apatites were dissolved in dilute warm HNO_3; zircon was dissolved using high-pressure digestion vessels. All isotopic ratios were measured on a Thermo Finnigan Element 2 sector ICP-MS following the routine of Reiners et al. (2004). A Fish Canyon Tuff zircon (28.48 ± 0.06 Ma; Schmitz and Bowring, 2001) and Durango apatite (31.4 ± 0.18 Ma; McDowell et al., 2005) were analyzed along with unknown aliquots. Alpha ejection correction followed Farley (2002) and Hourigan et al. (2005) for apatite and zircon, respectively.

Analytical uncertainties, which are a combination of measurement and systematic error, are commonly on the order of 1%–3% at the 2-σ level. Analytical error reflects the propagation of uncertainty from measurements of ^{4}He, U, Th, and Sm and grain size. The reported error does not take into account error associated with the alpha ejection correction, which in this study assumes a homogenous parent nuclide distribution within individual grains (Hourigan et al., 2005; Orme et al., 2015). The zircon He and apatite He data reported in Fig. 2 and in Appendix I and II are at the 2-σ level.

4.3. "Double-dating" with zircon U–Pb geochronology

A subset of eighteen zircon grains were "double-dated", applying both U–Pb geochronology and the (U–Th)/He method (Reiners, 2005; Carrapa et al., 2009) to further investigate the cooling history of detrital material preserved in the Xigaze forearc. This method is a powerful tool as it allows for recognition of syn-depositional volcanic grains (i.e. U–Pb and zircon He age are the same) and rapidly cooled grains. For the purposes of this study, this method is used to determine if the zircon He grains recorded post-depositional heating within the basin or source cooling events and whether or not cooling was associated with magmatism. Following Reiners (2005) and Fosdick et al. (2014), the data are reported as a plot of (U–Th)/He age versus U–Pb date (Fig. 3). Zircon U–Pb data from "double-dated" grains are available in Orme et al. (2015) and in Appendix I.

4.4. (U–Th)/He age variability

Known factors that contribute to age dispersion within the apatite and zircon He systems were investigated to determine the basin thermal history and to explain the observed age variability. Geologic factors that might play a role include sample stratigraphic position, elevation, and proximity to faults. Intrinsic properties of apatite and zircon, including grain size (Reiners and Farley, 2001), grain fragmentation (Brown et al., 2013), radiation damage (Shuster et al., 2006; Flowers et al., 2009; Gautheron et al., 2009; Guenthner et al., 2013), parent-nuclide zonation (Hourigan et al., 2005; Farley et al., 2011; Ault and Flowers, 2012; Gautheron et al., 2012; Johnstone et al., 2013; Orme et al., 2015) and He-implantation (Farley, 2002; Spiegel et al., 2009; Ketcham et al., 2011; Murray et al., 2014) must be considered to evaluate their contribution to age dispersion. I limited the effects of grain size and fragmentation during our analysis by picking only euhedral grains of similar size within a single sample suite. Back-scattered electron (BSE) images were obtained prior to U–Pb geochronologic analysis, revealing no evidence for pronounced chemical zonation in zircon grains. The potential affects of He-implantation are likely not a source of age variability as grains chosen for analysis were clear and lacked any visible grain boundary phases that may contribute excess parent or daughter nuclides (Murray et al., 2014). The effects of radiation damage on He diffusion kinetics, and therefore closure temperature, have highlighted the variability of the closure temperature window for apatite and zircon (Shuster et al., 2006; Flowers et al., 2009; Ketcham et al., 2011; Guenthner et al., 2013). In zircon, these effects are especially important for highly damaged grains (α-dose $>1.5 \times 10^{18}$ α/g), which may have closure temperatures less than the apatite He system (Guenthner et al., 2013; Johnson et al., 2013). The effects of radiation damage on He age are explored qualitatively and, during thermal modeling, quantitatively.

5. Results

5.1. Zircon (U–Th)/He

Thirty-seven zircon grains were analyzed for (U–Th)/He from forearc strata deposited between ~110 Ma and 54 Ma. Individual zircon He ages range from 31.5 ± 0.8 Ma to 6.1 ± 0.2 Ma, with the majority of grains yielding ages between 30 Ma and 10 Ma (Appendix I). The subset of eighteen double-dated zircons show a similar (U–Th)/He age range from 29.6 ± 0.8 Ma to 11.2 ± 0.3 Ma. Individual zircon He ages is plotted as a function of their depositional age in Fig. 2. In case of significant heating during deposition, the youngest zircon He age from a specific sample is expected to increase up section. However, within this dataset, two up-section trends are evident. First, samples from the Chongdoi and Ngamring formations show a decrease up section in the age of the youngest zircon from sample C_55 to sample G_197 (Fig. 2). Second, samples from the Padana to Jialazi formations show an up section decrease in the age of the youngest zircon from sample A_504 to sample G_23* (Fig. 2). There are no zircon He ages older than the

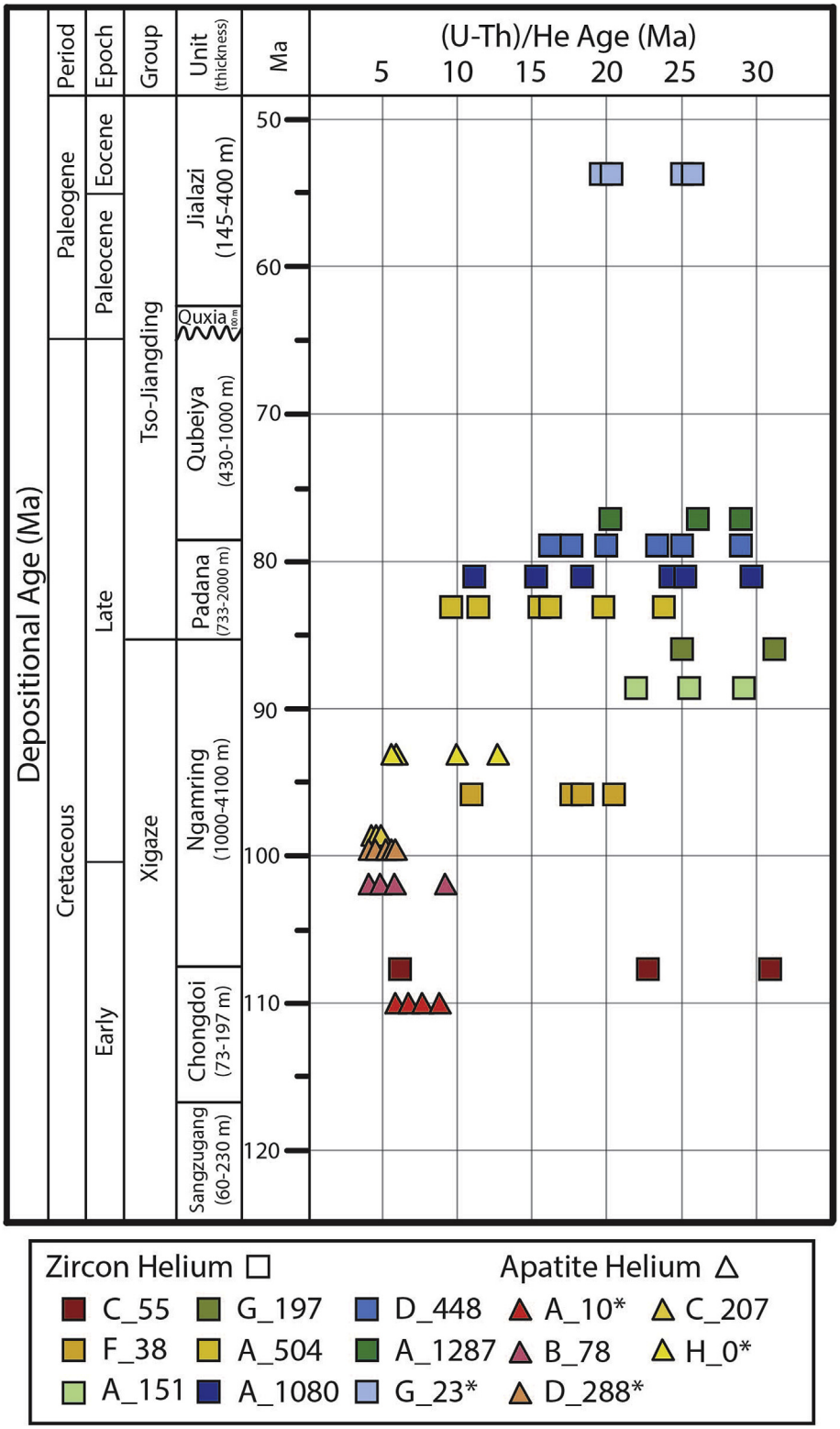

Figure 2. Apatite (triangles) and zircon (squares) (U–Th)/He ages as a function of sample depositional age and stratigraphic unit. Depositional ages from Orme et al. (2014) and Orme and Laskowski (2016). Tuff samples are denoted with an asterisk.

depositional age of the sample from which they are derived. Double-dating of individual zircon grains also yields zircon He ages significantly younger than their crystallization and depositional ages (i.e., 30–80 Ma younger), indicating at least partial resetting of the zircon He system (Fig. 3).

5.2. Apatite (U–Th)/He data

Twenty apatite grains were analyzed for (U–Th)/He from forearc strata deposited between ~110 Ma and 93 Ma. Individual apatite He ages range from 12.71 ± 0.50 Ma to 3.96 ± 0.28 Ma, with the

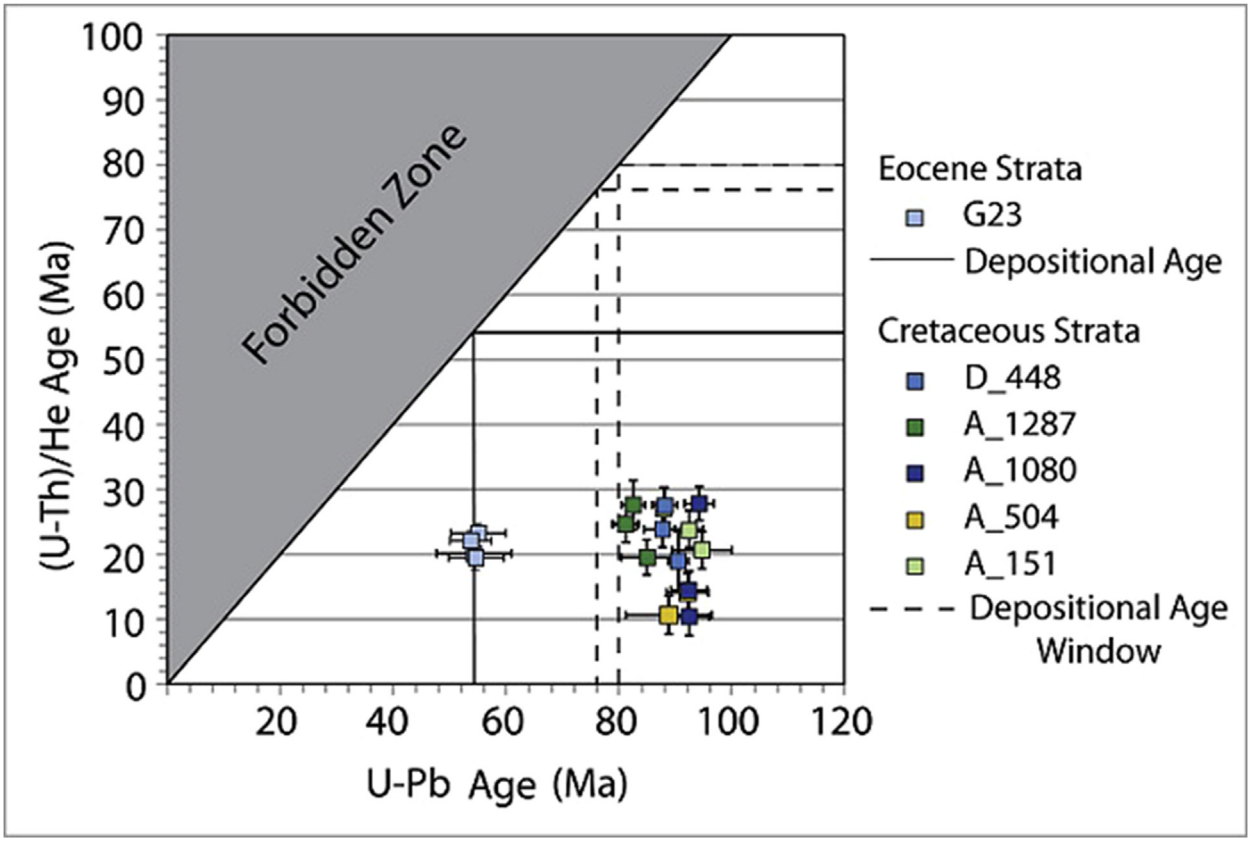

Figure 3. Individual double-dated ages from U–Pb and (U–Th)/He dating. The forbidden zone, as termed by Fosdick et al. (2014), is defined by the 1:1 line and indicates the region where no ages can exist as (U–Th)/He ages cannot be older than their crystallization age. (U–Th)/He ages from all samples are younger than their crystallization and depositional ages indicating that these samples are recording basin thermal processes, rather than source cooling histories.

majority of grains yielding ages between 9 Ma and 4 Ma (Appendix II). No correlation between stratigraphic position and apatite He age exists. Individual ages from a single-sample are within approximately 1–3 Ma of each other for samples A_10 (8.78 ± 1.37 to 5.84 ± 0.49 Ma), D_288 (5.81 ± 0.66 to 4.11 ± 0.53 Ma), and C_207 (4.91 ± 0.29 to 4.41 ± 0.36 Ma). Samples B_78 and H_0 show the largest intra-sample grain variability (>5 Ma) and yield the oldest apatite ages (Fig. 2). All apatite He ages are younger (i.e., >90 Ma younger) than their respective depositional age indicating temperatures >80 °C during burial and subsequent cooling post deposition.

6. Discussion

6.1. Interpretation of zircon and apatite (U–Th)/He data

Zircon and apatite He ages from Xigaze forearc samples are significantly younger than their respective depositional and crystallization ages (Figs. 2 and 3). This indicates that the Xigaze forearc was buried to temperatures high enough to reset the (U–Th)/He system in both apatite and zircon (>140 °C) and therefore record basin thermal processes rather than source exhumation. However, the zircon He age variation evident within individual samples (Fig. 2; Appendix I) suggests that the basin did not experience temperatures higher than >200 °C as this would likely produce fully-reset zircons that would display a tighter range of cooling ages. Thus, I interpret that these ages indicate that the samples were located in the partial retention zone for the zircon He system (140–200 °C) between 30 Ma and 10 Ma. Apatite He ages are fully reset and record cooling to <80 °C between 9 Ma and 4 Ma.

The two stratigraphic-age trends within the zircon He dataset are not interpreted to be geologically meaningful (Fig. 2). The first trend, from sample C_55 to sample G_197 is not geologically robust due to intrasample age variability. For example, the youngest single grain age from sample C_55 (6.06 ± 0.09 Ma) is ~16 Myr and ~24 Myr younger than the other two grains from the same sample. This grain has effective uranium concentrations of ~955 ppm, which is much higher compared to grains from the same sample that are <375 ppm (Fig. 4). It is possible that radiation damage may have exerted some control on the grain specific closure temperature, resulting in a significantly younger zircon He age (e.g., Guenthner et al., 2013). The second stratigraphic-age trend, from samples A_504 to G_23*, is also interpreted to be geologically meaningless due to intrasample grain variability and the lack of a trend between samples from the same stratigraphic succession (Fig. 2). Samples A_151 and A_504 were collected within a conformable stratigraphic sequence 353 m apart and expected to yield similar zircon He ages, with the overlying A_504 perhaps yielding slightly older single grain ages. Instead, the majority of single grain ages from sample A_504 are younger than the zircon He ages from sample A_151 (Fig. 2; Appendix I).

Additional factors that may contribute to age variability within the zircon He dataset likely exerted little control on the ages observed. The higher elevation samples were expected to have older cooling ages (Wagner and Reimer, 1972; Fitzgerald et al., 1993); however, there is no clear age-elevation correlation for either He system from each study region (Fig. 4A). Similarly, there is no correlation between age and distance from syncline axis (Figs. 1 and 4B).

It is unlikely that radiation damage exerted a primary control on He age variation, as the corresponding U–Pb crystallization

ages are relatively young (<110 Ma), limiting the amount of time for radiation damage accumulation. Nevertheless, effective uranium concentration (eU = 0.235Th + U) was used as a proxy for radiation damage because negative or positive age-eU correlations can provide information on a sample's thermal history by revealing radiation-damage driven changes in closure temperature (Shuster et al., 2006; Flowers et al., 2009; Gautheron et al., 2009; Guenthner et al., 2013). Zircon from individual samples show either slight negative or positive age-eU correlations, or no correlation. Considering all 37 single-grain zircon He ages together reveals no clear age-eU correlation (Fig. 4C). Apatite from the entire dataset display no age-eU correlation (Fig. 4D). Based on this analysis, radiation damage was excluded as a significant control on the observed age variability within the samples. Thus, the spread of zircon He ages is interpreted to reflect sample variations in maximum burial temperature within the partial retentation zone for the zircon He system (~140–200 °C).

6.2. Thermal modeling

6.2.1. Single sample: apatite He, Lazi

Thermal modeling investigates if the interpreted burial temperatures and cooling history are consistent with the observed data. Inverse modeling using the HeFTy program (Ketcham, 2005), which is based on a Monte-Carlo algorithm that takes into account both diffusive loss and radiogenic ingrowth of He for individual grains as a function of their thermal history, was used to test a range of thermal histories that might provide good fits to the data. Modeling first focused on Sample A_10, a tuffaceous unit deposited in the basin at 110 Ma in the Lazi region (Fig. 1). Using this sample allows for isolation of the thermal history of the basin, without inclusion of an earlier *t–T* history (detrital signature) required for grains sourced from Gangdese arc plutons. In addition, focusing on this sample provided an opportunity to evaluate the stratigraphically deepest parts of the Xigaze forearc basin, which likely records maximum burial temperatures.

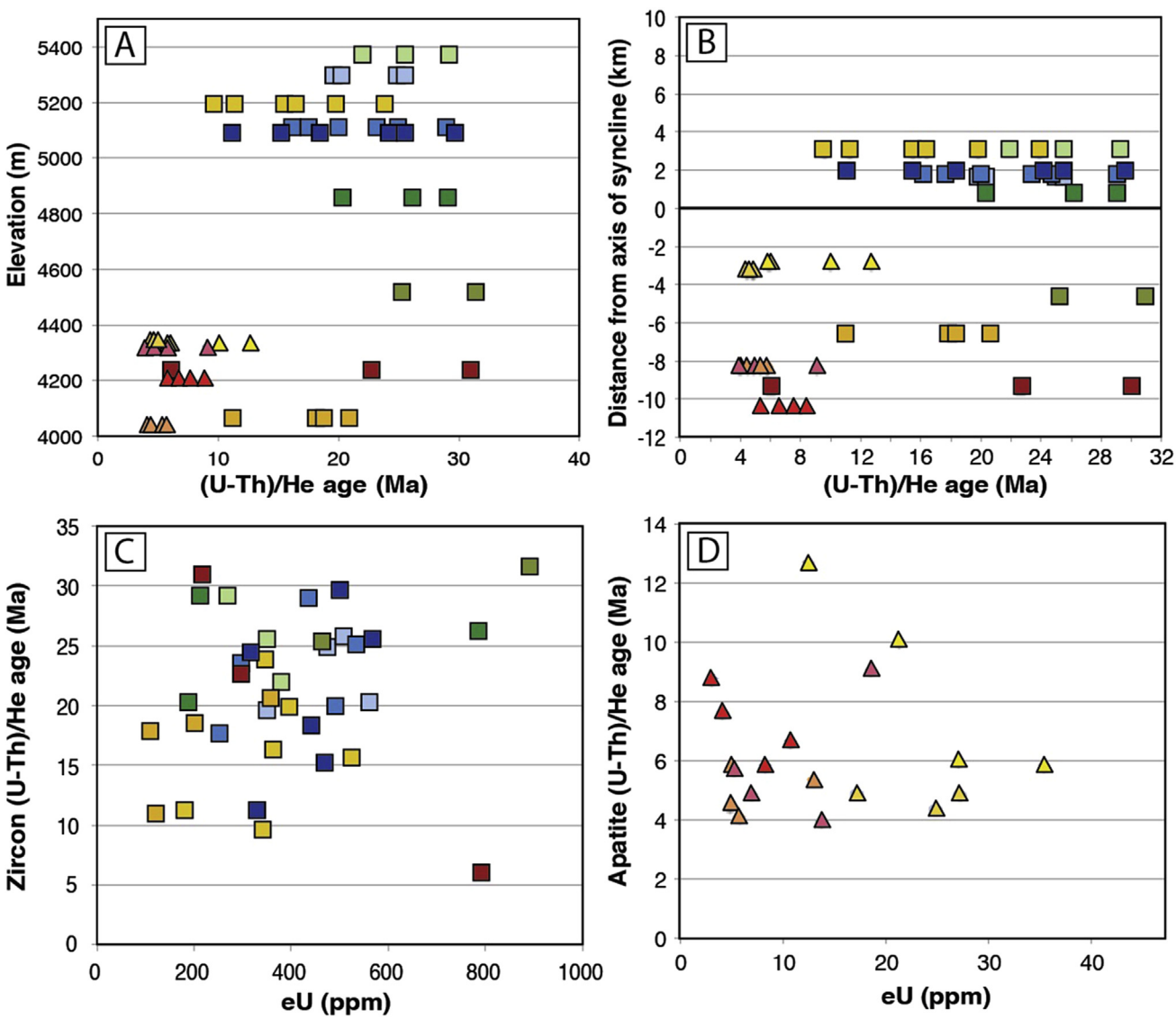

Figure 4. (A) Elevation versus (U–Th)/He age, showing no correlation. (B) Structural position within the Xigaze forearc basin syncline versus (U–Th)/He age. (C) and (D) zircon and apatite (U–Th)/He age as a function of effective uranium (eU = 0.235Th × U). Symbols are the same as Fig. 2.

The searchable *t*–*T* space for the thermal history paths was defined using the following five input parameters (Fig. 5A), expressed graphically in Fig. 5 as boxes through which *t*–*T* paths were forced:

(a) Sample A_10 was deposited at the surface between 0 and 20 °C at 110 Ma.
(b) There is at least 2453 m of stratigraphic thickness preserved above sample A_10 in the Lazi region (Orme and Laskowski, 2016). Assuming a depressed geothermal gradient of 20 °C/km (e.g., Dumitru, 1991), consistent with typical geothermal gradients in a forearc setting, this sample must have been buried to at least 50–70 °C by 86 Ma—the age of the youngest sample deposited and preserved in the Lazi region.
(c) Zircon He ages from the Lazi region between ~31 Ma and 6 Ma require burial to 140 and 200 °C, within the zircon He partial retention zone (140–200 °C).
(d) Sample A_10 was at temperatures of 40–80 °C between 8 Ma and 5 Ma based on the Apatite He ages (Fig. 2).
(e) Sample A_10 was collected at the surface (0–20 °C) at 0 Ma.

The time-interval between 86 Ma and 30 Ma is largely unconstrained by the five input parameters. This is in part due to the lack of sedimentary strata preserved during this interval. For instance, although >3 km of strata deposited between 86 Ma and 51 Ma are found in the Saga region (Orme et al., 2015), these are not preserved or may have not been deposited in the Lazi region (Fig. 5C). In addition, following onset of collision at ca. 58 Ma (Garzanti et al., 1987; DeCelles et al., 2014) and cessation of forearc sedimentation at ca. 51 Ma (Hu et al., 2015; Orme et al., 2015), there is no sedimentary record in the YSZ until deposition of the Kailas Formation between 26 Ma and 18 Ma (Fig. 5C; Einsele et al., 1994; DeCelles et al., 2011; Leary et al., 2016). In addition, motion across forearc basin bounding faults (GCT system) did not initiate until ~25 Ma (Quidelleur et al., 1997; Yin et al., 1999). Despite the fact that the zircon He ages requires burial to >140 °C, but <200 °C prior to ~30 Ma, there is no geologic evidence of the rocks that were responsible for this burial.

The *t*–*T* paths resolved by the HeFTy thermal model are in Fig. 5B as a series of good and acceptable fit paths, along with the weighted mean of the good fit paths. The weighted mean path shows a *t*-–*T* history that allows the sample to linearly heat until cooling, as recorded by the zircon He data, initiating by ~20 Ma. In contrast, the good and acceptable fit paths suggest a series of complex heating histories between 86 Ma and 30 Ma prior to primarily linear cooling. The majority of good and acceptable fits for the zircon He data require the sample to have reached maximum temperatures of <200 °C between 30 Ma and 20 Ma, but no later than ~20 Ma. Cooling of the basin initiated immediately following peak heating temperature between ~30 Ma and 20 Ma and appears to be monotonic below ca. 60 °C between 8 Ma and 5 Ma.

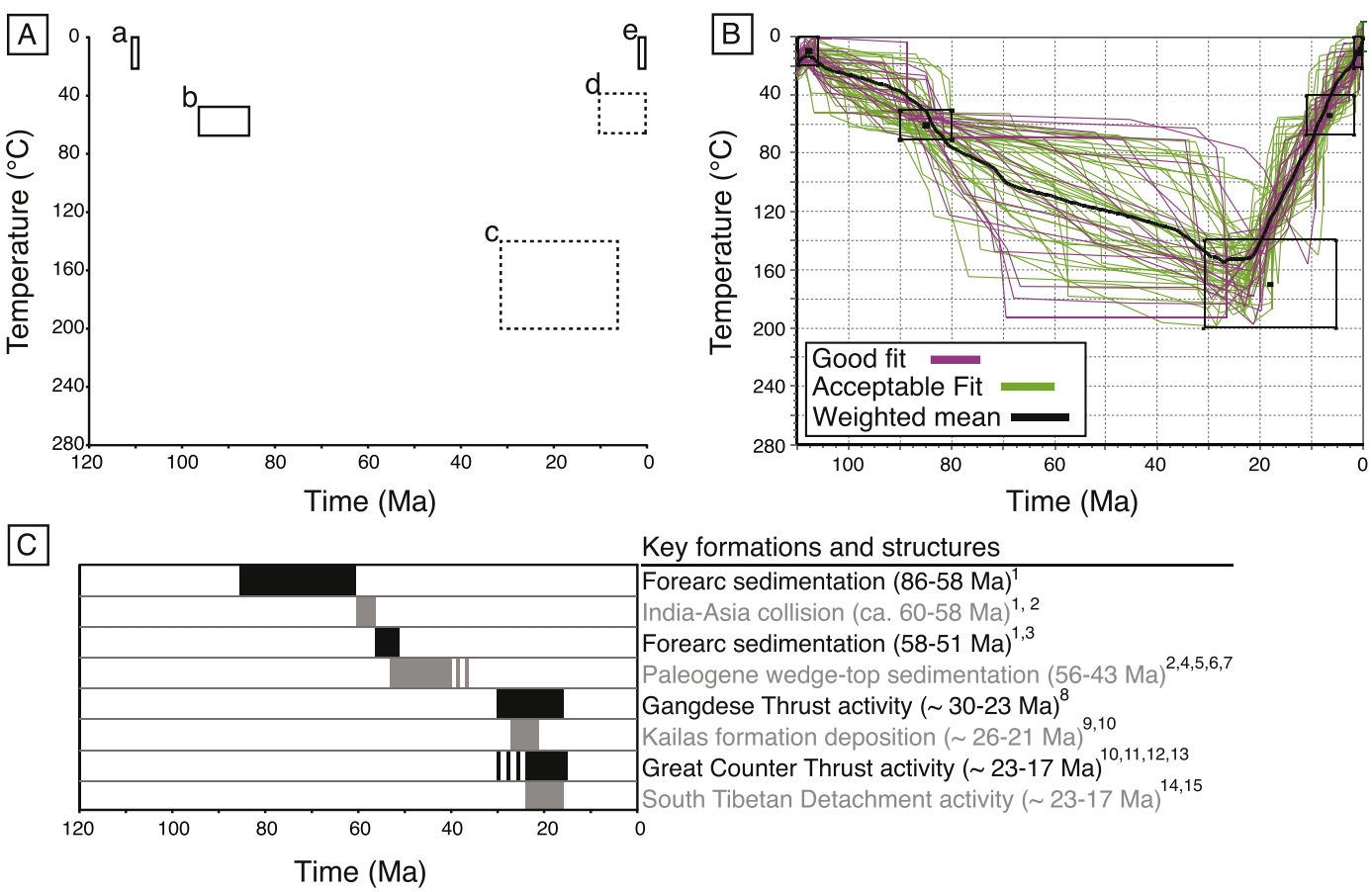

Figure 5. (A) Model set-up following the five input parameters described in the text. Dashed boxes are defined by He data. Solid boxes defined by stratigraphic evidence. (B) Good and acceptable model fits. (C) Key sedimentary formations deposited and structures active during the least constrained period of heating between ~86 Ma and 26 Ma and cooling between ~20 Ma and 15 Ma. 1: Orme et al. (2015); 2: DeCelles et al. (2014); 3: Hu et al. (2015); 4: Najman et al. (2010); 5: Zhang et al. (2012); 6: Hu et al. (2012); 7: Zhu et al. (2005); 8: Yin et al. (1994); 9: DeCelles et al. (2011); 10: Leary et al. (2016); 11: Quidelluer et al. (1997); 12: Yin et al. (1999); 13: Laskowski et al. (2017); 14: Hodges et al. (1998); 15: Murphy and Harrison (1999).

Please cite this article in press as: Orme, D.A., Burial and exhumation history of the Xigaze forearc basin, Yarlung suture zone, Tibet, Geoscience Frontiers (2017), https://doi.org/10.1016/j.gsf.2017.11.011

6.2.2. Multiple samples: Lazi and Saga

The inverse and forward thermal-history modeling abilities of the software program QTQt (Gallagher, 2012) were utilized to investigate further the apatite He data and complexity of the zircon He data. This program uses a Bayesian transdimensional approach to data inversion, where a defined model space is sampled using a Markov chain Monte Carlo method. Modeling in QTQt is particularly useful for large datasets where the variability in ages prevents averaging of grain-specific inputs and the addition of more data improves the resolution of the *t–T* history (Vermeesch and Tian, 2014). First, inverse thermal models were explored for apatite and zircon He samples from the Lazi region. Following the best-fit *t–T* paths from the inverse models, forward modeling was used to find a best fit for zircon He samples from the Saga region.

In the Lazi region, sixteen individual grains from four apatite He samples (A_10*, B_78, D_288, H_0) were modeled in aggregate to investigate the extent of heating and timing of regional cooling (Appendix III). Sample C_207 was excluded from the model as it is located in the footwall of a mapped normal fault and yields a cluster of very young ages (~4 Ma). The model inputs are grain specific and include the raw age and error, grain composition (U, Th, Sm, He), and grain dimension (length, width, height). The model utilized the RDAAM model (Flowers et al., 2009) to quantify the effects of grain chemistry and cooling rate on closure temperature. Thermal histories were only constrained by the depositional age and current surface temperature at the sample location (~10 °C), with a maximum temperature range of 0–200 °C explored. All input parameters are summarized in Appendix III. The thermal model outputs from the Bayesian inversion are shown as a mean thermal history model, termed the "expected model" (weighted by the posterior probability of each individual thermal history), and include 95% confidence intervals (Fig. 6). The model output also compares individual grain ages predicted by the expected model with the observed data; this comparison was used to test the ability of the model to reproduce the observed He age data.

The thermal model from the inversion of apatite He data from the Lazi region that best reproduces the observed mean ages indicates maximum burial temperatures for the stratigraphically lowest (blue lines) and highest samples (red lines) of 100–125 °C and 140–170 °C by ~35–33 Ma, respectively. The model indicates that cooling (exhumation) began between 33 Ma and 30 Ma, with an increased rate to reach temperatures ≤ 40 °C at ~4 Ma (Fig. 6A). The expected thermal history predicts apatite He ages within error of the observed ages (Fig. 6B). Given the large range of the 95% confidence intervals for the timing of cooling, zircon He data were integrated to further constrain the thermal history.

Modeling apatite He and zircon He data together proved challenging owing to the temporal, spatial (elevation), and stratigraphic variability of the samples as compared with the apatite He samples. No sample has both apatite and zircon He dates, but zircon He sample (F_38) was integrated with the apatite He dataset because it was located geographically and stratigraphically closest to the apatite He samples and displayed limited age variability (Fig. 6D). The *t–T* history that best reproduced the apatite He and zircon He observed ages allowed the stratigraphically deepest samples to heat along an about linear path to maximum burial temperatures of 175–200 °C just prior to the onset of cooling at ~21–20 Ma (Fig. 6C). Cooling is approximately linear between 21 Ma and 8 Ma, followed by an apparent cessation of cooling prior to a rapid decrease in temperature from 4 Ma to the present (Fig. 6C). The *t–T* model predicts apatite and zircon He ages within the 95% probability range, but the observed apatite He ages are consistently younger than the predicted ages from the model. The segment of the cooling path between 21 Ma and 8 Ma is the most tightly constrained (i.e., the 95% probability contours are close together), whereas the period between ~90 Ma and 30 Ma is the least constrained. Nevertheless, the best-fit model predicts continuous heating until 21 Ma, similar to the *t–T* histories of the apatite He only model (Fig. 6A) and the thermal history predicted by the tuffaceous sample A_10*(Fig. 5B). Interestingly, the inverse model involving only apatite He data from Lazi region (Fig. 6A) suggests similar burial temperatures to those predicted by the model that incorporates zircon He data.

In the Saga region, nineteen individual grains from six zircon He samples (A_151, A_504, A_1080, A_1287, D_448, G_23*) were modeled together using the forward modeling abilities of QTQt. Double-dated grains were excluded from the model as grain specific U–Pb ages cannot be integrated into the model without introducing excessive complexity. In addition, inclusion of these grains biases the dataset as double-dated samples have twice the number of grains compared to the other samples. Forward modeling was used to explore the same *t–T* space as the inverse models, with the timing and magnitude of maximum burial and cooling varied systematically. The forward model starts at the mean depositional age of the five Cretaceous samples (80 Ma) and buries the deepest samples prior to the onset of heating of the stratigraphically lowest sample (G_23*) following deposition ca. 54 Ma. The temperature offset between the lowest and highest stratigraphic samples is held constant at 20 °C during heating and initial cooling; the temperature offset during the final stages of cooling is removed as the model forces the samples to surface temperature at 0 Ma. Burial temperatures of 140–220 °C between 30 Ma and 10 Ma were explored. The timing of initial cooling from those temperatures was also explored between 30 Ma and 10 Ma. Initial cooling paths tested immediate cooling following peak burial temperatures and holding the samples at maximum burial temperatures for 5, 10, 15 or 20 Myr.

The best-fit forward model reproduced 12 of the 19 zircon He ages within 1σ error (Fig. 7). The model indicates that heating was linear until maximum burial to temperatures of 180–200 °C by ~21 Ma, beginning with deposition of the stratigraphically lowest sample (G_23*) at 53.8 ± 0.7 Ma (Fig. 7A). The onset of cooling immediately followed maximum burial and is rapid until ~15 Ma where cooling slowed down between 40–60 °C and 0 °C (surface temperature). Paths which assume linear cooling from 21 Ma to 0 Ma, reproduce less ages than *t–T* paths which decrease cooling rate ca. 15 Ma (Fig. 7B).The decrease in cooling rate coincides with ~17 Ma onset of extension along the Lopu Range bounding normal fault, the Rujiao fault, 10 km to the southwest of the forearc in the Saga region (Laskowski et al., 2017). Xigaze forearc strata are located in the hanging wall of the Rujiao fault, which was active since at least ~17 Ma, with more recent motion likely, as evidenced by triangular facets (Laskowski et al., 2017). Therefore, a decrease in the rate ca. 15 Ma is consistent with the regional geology.

6.3. Regional tectonic implications

6.3.1. Xigaze forearc burial

Thermochronologic data reported in this study, supported by thermal-kinematic modeling results, indicate that the stratigraphically deepest parts of the Xigaze forearc basin were heated to 140–200 °C (~5–8 km in depth), which is not attainable by the preserved forearc stratigraphic thickness alone. A possible candidate for further heating is burial of the forearc by a forearc successor basin with sedimentation during the Paleogene. South of the YSZ, there are a series of Paleogene stratigraphic sections preserved in the Sangdanlin and Tingri regions that are interpreted to have been deposited in a foredeep or wedge-top position during early development of the nascent Tethyan Himalayan thrust belt and foreland basin system (Fig. 1; Zhu et al., 2005; Najman et al., 2010; Wang et al., 2011; Zhang et al., 2011; Hu et al., 2012; DeCelles et al.,

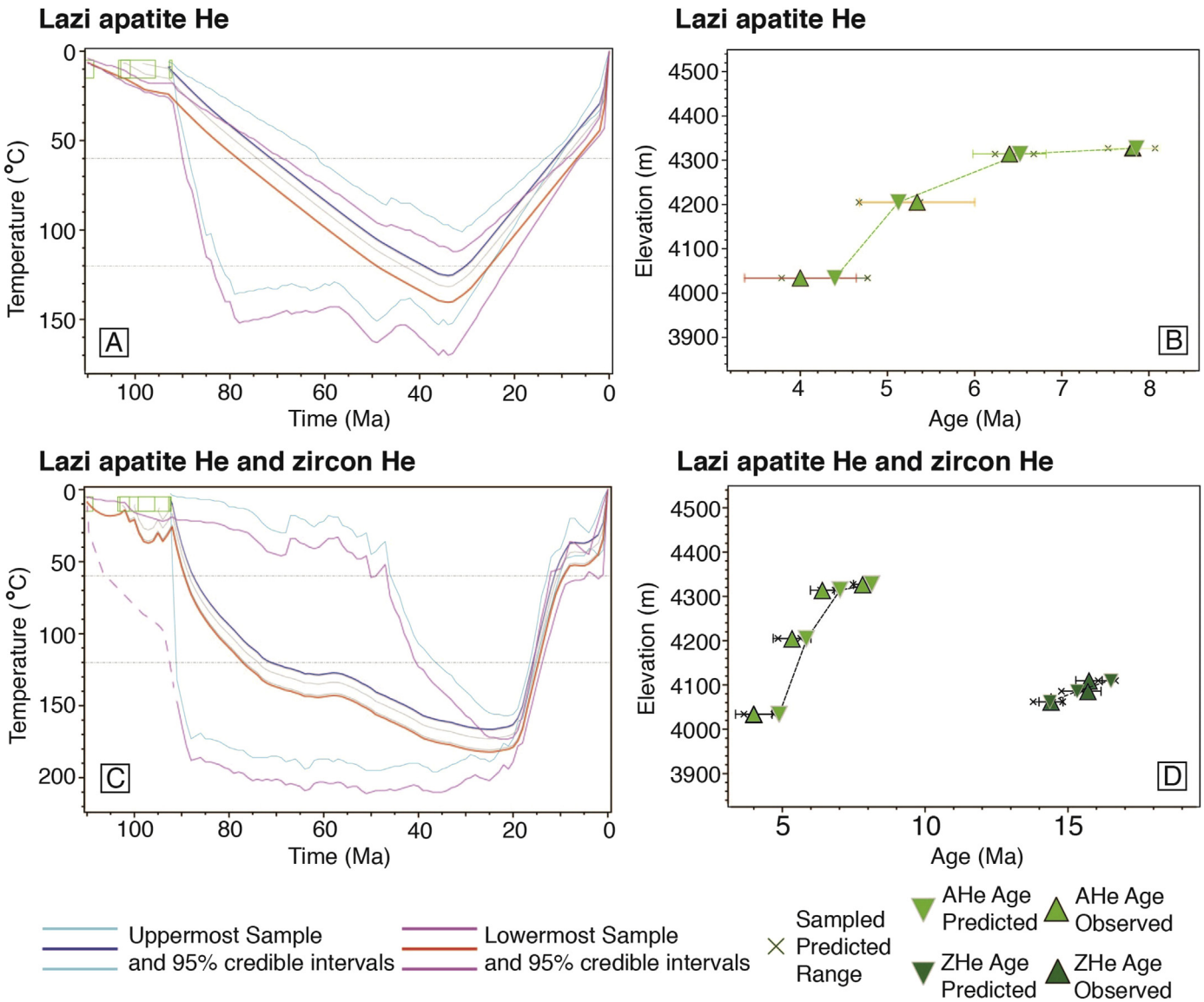

Figure 6. (A) Inverse thermal modeling results for four apatite samples from the Lazi region. The stratigraphically highest (uppermost) are in blue and the lowest (lowermost) samples are in red. Grey lines are intermediate samples (B) predicted and observed apatite He ages from Lazi as a function of sample elevation; dashed line is the best fit between predicted ages. (C) Inverse thermal modeling results for four apatite samples and one zircon sample from the Lazi region. Cooling from maximum temperatures of 170–200 °C from 21 Ma to 8 Ma is tightly bracketed as compared to the heating between 86 Ma and 22 Ma. (D) Predicted and observed He ages from the Lazi region; all ages overlap with 95% confidence.

2014). In the Tingri region, the Zhaguo Formation, which is 75 m-thick, is interpreted as a series of fluvial channel and floodplain facies sourced from the north and deposited in a wedge-top environment between ~50 Ma and 43 Ma (Zhu et al., 2005; Najman et al., 2010; Hu et al., 2012). The lower age limit on sedimentation is disputed, and it is plausible that wedge-top sedimentation in Tingri extends to as young as ~35 Ma (Wang et al., 2002).

In the Saga region of the Xigaze forearc, the 400 m-thick Jialazi Formation is interpreted as a syn-collisional unit deposited atop forearc strata during the initial stages of collision from ~58 Ma to 54 Ma (Hu et al., 2015; Orme et al., 2015). The Jialazi Formation may extend to younger than 54 Ma, as this age is a maximum depositional determined from detrital zircon U–Pb geochronology (Hu et al., 2015; Orme et al., 2015). I hypothesize that the Jialazi Formation is a remnant of a Paleogene forearc successor basin, a foreland wedge-top basin, similar to the Zhaguo Formation near Tingri. The heating constraints from the zircon He suggest that this basin may have been ~1 km thick, which is similar to documented thicknesses in other basins that sit in a wedge-top setting (e.g., Ricci Lucchi, 1986; Coogan, 1992; DeCelles, 1994). This hypothesis would be supported if unconformities within the Jialazi, growth structures, or regional thinning towards orogenic wedge are present (DeCelles and Giles, 1996). However, these characteristics are challenging to identify in the field owing to deformation and incision of Xigaze forearc strata. Nevertheless, the textural and compositional immaturity of the Jialazi deposits are consistent with deposition in a wedge-top setting. Interestingly, magmatism within the Gangdese arc continued until ~38 Ma (Kapp et al., 2008) and magmatic addition may have further driven topographic relief of the arc region and contributed to the creation of accommodation space in the forearc region. The magmatic arc activity could provide a source of detritus for the foreland wedge-top basin, thus making it hard to petrographically and geochemically differentiate between the forearc basin and the successor wedge-top basin.

Burial of the forearc by a wedge-top basin requires no additional heating from deposition of the Kailas Formation between 26 Ma and 21 Ma (DeCelles et al., 2011; Carrapa et al., 2014; Leary et al., 2016). DeCelles et al. (2011) interpreted the southern limit of the Kailas basin during deposition to be a steep north-dipping normal fault. This interpretation is supported by the presence of Gilbert deltas and paleocurrent indicators along the southern belt of facies at its type locality (DeCelles et al., 2011). If this interpretation is correct, then Kailas Formation strata could not have buried Xigaze forearc basin strata. In addition, the north-directed northern splay of the GCT, located along the southern margin of the Kailas basin, is structurally below the Xigaze forearc and therefore structurally buries the Kailas Formation (Yin et al., 1999; DeCelles et al., 2011).

6.3.2. Xigaze forearc exhumation

Zircon He ages between ~30 Ma and 10 Ma indicate that basin cooling initiated during this time, but the variability of the ages caused by partial-resetting during basin heating precludes the possibility of narrowing the estimate using the ages alone. However, thermal-kinematic modeling suggests that the basin began to exhume at ~21–15 Ma (Figs. 6C and 7A). The timing of this event is coincident with Late Oligocene to Early Miocene cooling documented in the Gangdese magmatic arc, which is attributed to denudation during south-directed displacement along the Gangdese thrust (Copeland et al., 1987; Yin et al., 1994; Harrison et al., 2000; Dai et al., 2013; Li et al., 2015). In addition, timing is concurrent also with Early Miocene cooling of the Kailas Formation, attributed to efficient paleo-Yarlung River incision (Carrapa et al., 2014). Although the Gangdese thrust is not documented in the two regions of study, if it was active at this time it would structurally bury the Xigaze forearc, not exhume it.

The onset of exhumation of the Xigaze forearc between 21 Ma and 15 Ma coincides with proposed movement across the GCT system, constrained to ~25–17 Ma, based on crosscutting relationships between the GCT and the Gangdese thrust to the north (Quidelleur et al., 1997; Yin et al., 1999; Harrison et al., 2000) and the GCT and north-striking normal faults (Laskowski et al., 2017). The northern splay of the GCT system cannot explain coeval exhumation of the forearc and Kailas basins as it structurally buries the Kailas Formation (Carrapa et al., 2014). In addition, the thermochronologic results herein have implications for the timing of movement along the southern splay of the GCT, bounding the southern margin of the forearc. As this fault structurally buries the southern part of the basin where the majority of the samples record cooling at ~21–15 Ma, motion across the fault likely ceased or became low-magnitude prior to this time to allow for footwall cooling. Mean AFT cooling ages of ~17 Ma from the Kailas basin and crosscutting relationships in the Saga region (Laskowski et al., 2017) suggests cessation of thrusting along the GCT at a similar time, by ~17 Ma.

As the Late Oligocene to Early Miocene thermochronometric signal appears to be regionally extensive throughout different lithotectonic units of the YSZ, any model that seeks to explain the exhumation of the Xigaze forearc must also be consistent with this regional signal. The GCT system may have contributed to the development of structural relief and topographic growth within the forearc region. However, based on timing constraints for motion across the GCT system, movement must coincide with enhanced regional erosion to drive exhumation and be consistent with coeval exhumation across different lithotectonic units of the YSZ. Possible mechanisms that may have increased erosion rates along the IYSZ at this time include efficient river incision by a paleo-Yarlung River related to capture by the Brahmaputra River (Cina et al., 2009; Robinson et al., 2013; Carrapa et al., 2014, 2017; Lang and Huntington, 2014) or intensification of the Asian monsoon (Quade et al., 1989; Clift et al., 2008). This study hypothesizes that Early Miocene exhumation of the YSZ was driven by enhanced rock uplift across the GCT system, which resulted in heightened erosion by the paleo-Yarlung-Brahmaputra river system. An integrated Yarlung-Brahmaputra river system in the Miocene, which would enhance erosion and evacuation of material from the suture zone, is supported by the appearance of Gangdese magmatic arc derived zircons in Early Miocene foreland basin deposits along the eastern Himalayan syntaxis (Lang and Huntington, 2014) and Central Myanmar Basin (Robinson et al., 2013). As proposed by Carrapa et al. (2017), the regional uplift-induced erosion and coupled river incision may have been a response to renewed underthrusting of India beneath Asia, following a period of rollback (DeCelles et al., 2011). Intensification of the Asian monsoon as a possible driver for exhumation in Miocene time is difficult to test, in part due to patterns of modern cooling ages along the suture zone. If the modern monsoon was solely responsible for exhumation of the region, one would predict young (≤Pliocene) cooling ages across the entire suture zone. However, young (≤Pliocene) cooling ages are restricted to active rifts or the Himalayan syntaxes (e.g., Styron et al., 2015; Lang et al., 2016). Thus, the effects of the monsoon on erosion patterns in the Miocene are challenging to reconstruct using thermochronology alone.

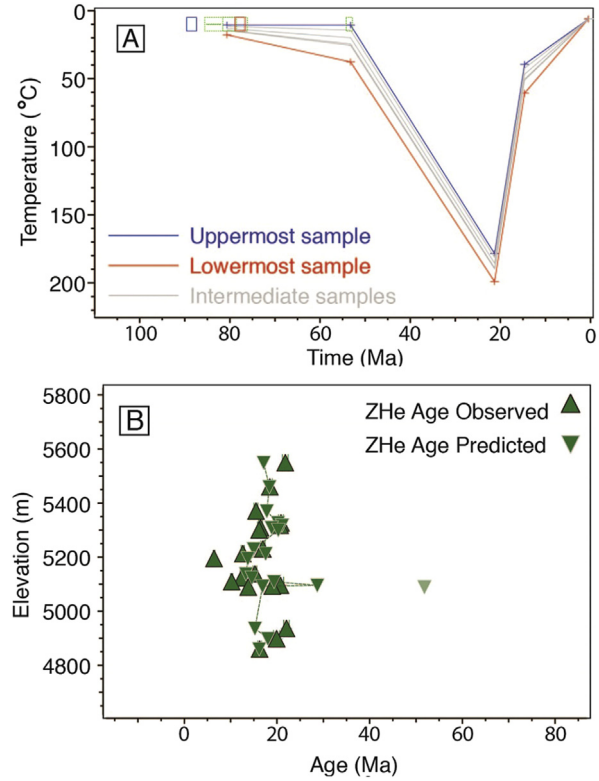

Figure 7. Forward thermal modeling results for six zircon samples from the Saga region (A) and the predicted ages as compared to observed ages (B). Maximum heating is to 180–200 °C by ~21 Ma, followed by a slowing of cooling rate between 15 Ma and 0 Ma.

The apatite and zircon He thermochronologic dataset presented in this study determine how much material was removed since the onset of exhumation between 21 Ma and 15 Ma. Using a geothermal gradient of 25 °C/km, zircon He and apatite He ages suggest cooling from a mean temperature of 160 °C and 60 °C, respectively, requiring removal of ~4 km of material from across the Xigaze forearc region between ~21 Ma and ~8 Ma and an additional 2.4 km of material since ~8 Ma (Figs. 5–7). The Late Miocene to

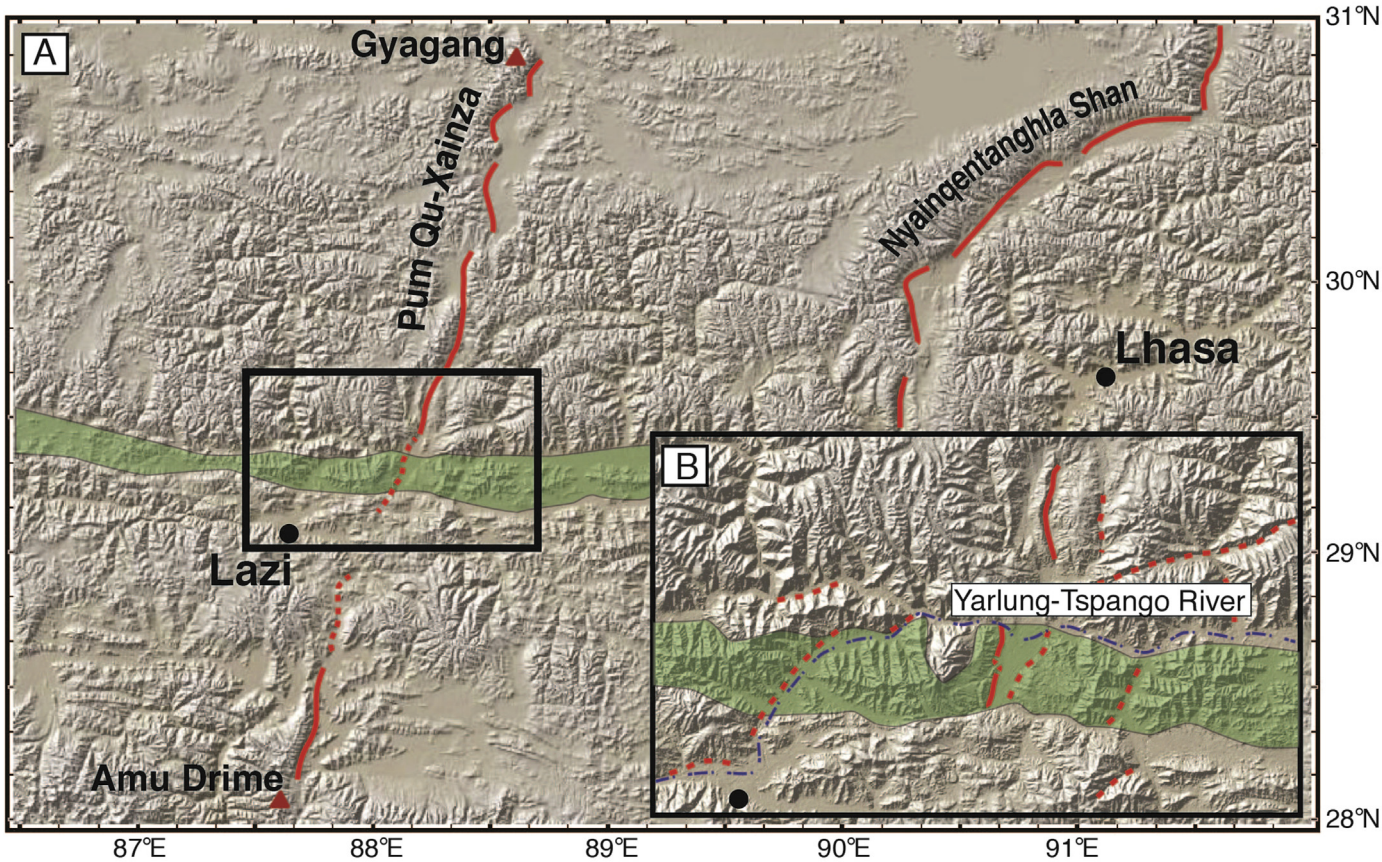

Figure 8. (A) Digital elevation model (DEM) showing the distribution of major N-S trending rift structures Pum Qu-Xainza and Nyainqentanghla, modified after Taylor and Yin (2009). (B) DEM of region B (Lazi field area) with interpreted active normal faults cross-cutting the Xigaze forearc. The Xigaze forearc basin is shown in green. Digital elevation shaded relief base map from Global Multi-Resolution Topography Synthesis.

Early Pliocene cooling event recorded by the apatite He ages (12–4 Ma) is coeval with documented cooling from 11 Ma to 8 Ma in the Gangdese magmatic arc near Lhasa (Copeland et al., 1987; Dai et al., 2013) and 9–4 Ma cooling documented in the Kailas Formation at Mt. Kailas (Carrapa et al., 2014).

The timing of Late Miocene to Early Pliocene exhumation within the forearc is coincident with the onset of orogen-parallel extension by 16 Ma and accelerated exhumation ca. 8–4 Ma along structures that cross-cut the YSZ (Sundell et al., 2013 and references therein; Laskowski et al., 2017). In the Lazi region, apatite He samples yield mean cooling ages <8 Ma, consistent with cooling associated with regional normal faults. A north-trending rift, proximal to the Lazi region, is the Pum Qu-Xainza rift, ~20 km to the northeast of the Lazi field area (Fig. 8A; Hager et al., 2009; Taylor and Yin, 2009). Estimates for the timing of extension along this rift suggest initiation of exhumation at 14 Ma, followed by a second stage at 8 Ma (Hager et al., 2009). Taylor and Yin (2009) map this fault as crosscutting the YSZ at the latitude of Lazi. Detailed structural mapping of system in the Lazi region is limited, but field observations and remote mapping of satellite imagery reveals a series of fault scarps that trend northeast (Fig. 8B). Apatite He sample C_207, collected in the footwall of one of these faults, yields three cooling ages of 4.41 ± 0.36, 4.88 ± 0.25, and 4.91 ± 0.29 Ma. The ~4 Ma cooling signal is consistent with accelerated cooling documented in the footwalls of active normal faults north of the YSZ (Sundell et al., 2013; Styron et al., 2015), and is the first documented cooling signal of similar age along the central part of the YSZ to date. In the Lazi region, incision of the Yarlung River is likely enhanced as it responds to footwall exhumation, contributing to the net exhumation of the region.

7. Conclusions

(1) Zircon He data indicate that the stratigraphically deepest parts of the Xigaze forearc were buried to ~120–135 °C by 51 Ma, which corresponds to depths attainable by forearc sedimentation. Following the onset of collision and cessation of forearc deposition, the zircon He data require an additional burial to 140–200 °C, which may be achieved by sedimentation in a Paleogene forearc successor basin (i.e., foreland wedge-top basin).

(2) Zircon He and apatite He results indicate exhumation in Early Miocene time (~21–15 Ma), followed by additional cooling in Late Miocene to Early Pliocene time (~4 Ma). The 21–15 Ma thermochronometric signal is regionally extensive, affecting all the lithotectonic units of the YSZ and coincides with movement along the north-vergent Great Counter Thrust system. Thrusting, coupled with enhanced erosion possibly related to the paleo-Yarlung River, likely drove Early Miocene cooling of the Xigaze forearc basin.

(3) Apatite He ages record footwall cooling along proximal north-south trending rifts that crosscut the YSZ. Motion along these faults likely enhanced local down cutting of the Yarlung River, which contributes to the net exhumation of the region.

Please cite this article in press as: Orme, D.A., Burial and exhumation history of the Xigaze forearc basin, Yarlung suture zone, Tibet, Geoscience Frontiers (2017), https://doi.org/10.1016/j.gsf.2017.11.011

Acknowledgements

Barbara Carrapa, Paul Kapp, Peter G. DeCelles, and Andrew K. Laskowski are thanked for informative discussions on the regional geology. Peter W. Reiners is appreciated for insightful conversations on the (U–Th)/He dataset and Uttam Chowdhury for assistance with zircon (U–Th)/He analytical work. D.A. Orme is very grateful to Dr. Lin Ding for help obtaining research permits and support to work in the region. Delores Robinson, Aaron J. Martin, and Associate Editor Dr. Christopher Spencer are appreciated for detailed reviews that improved the quality of this publication. This research was supported by the U.S. National Science Foundation Continental Dynamics Program (EAR-1008527; Lead PI, P. Kapp). All data reported in this manuscript are available in Appendices I and II.

Appendix A. Supplementary data

Supplementary data related to this article can be found at https://doi.org/10.1016/j.gsf.2017.11.011.

References

Allègre, C.J., Courtillot, V., Tapponnier, P., Hirn, A., Mattauer, M., Coulon, C., Jaeger, J.J., Achache, J., Scharer, U., Marcoux, J., Burg, J.P., Girardeau, J., Armijo, R., Gariepy, C., Gopel, C., Li, T., Xiao, X., Chang, C., Li, G., Lin, B., Teng, J., Wang, N., Chen, G., Han, T., Wang, X., Den, W., Sheng, H., Cao, Y., Zhou, J., Qiu, H., Bao, P., Wang, S., Wang, B., Zhou, Y., Xu, R., 1984. Structure and evolution of the Himalaya-Tibet orogenic belt. Nature 307, 17–22.

An, W., Hu, X., Garzanti, E., Boudagher-Fadel, M.K., Wang, J., Sun, G., 2015. Xigaze forearc basin revisited (South Tibet): provenance changes and origin of the Xigaze Ophiolite. Geological Society of America Bulletin 126, 1595–1613.

An, W., Hu, X., Garzanti, E., 2017. Sandstone provenance and tectonic evolution of the Xiukang Mélange from Neotethyan subduction to India-Asia collision (Yarlung-Zangbo suture, south Tibet). Gondwana Research 41, 222–234.

Ault, A.K., Flowers, R.M., 2012. Is apatite U-Th zonation information necessary for accurate interpretation of apatite (U-Th)/He thermochrnometry data? Geochimica et Cosmochimica Acta 79, 60–78.

Bracciali, L., Najman, Y., Parrish, R.R., Akhter, S.H., Millar, I., 2015. The Brahmaputra tale of tectonics and erosion: Early Miocene river capture in the Eastern Himalaya. Earth and Planetary Science Letters 415, 25–37.

Brown, R.W., Beucher, R., Roper, S., Persano, C., Stuart, F., Fitzgerald, P., 2013. Natural age dispersion arising from the analysis of broken crystals, part I. Theoretical basis and implications for the apatite (U-Th)/He thermochronometer. Geochimica et Cosmochimica Acta 122, 478–497.

Burg, J.P., Chen, G.M., 1984. Tectonics and structural zonation of southern Tibet, China. Nature 311, 219–223.

Cai, F., Ding, L., Leary, R.J., Wang, H., Xu, Q., Zhang, L., Yue, Y., 2012. Tectonostratigraphy and provenance of an accretionary complex within the Yarlung-Zangpo suture zone, southern Tibet: insights into subduction-accretion processes in the Neo-Tethys. Tectonophysics 574–575, 181–192.

Carrapa, B., Hassim, M.F.b., Kapp, P., Gehrels, G.E., 2017. Detrital geochemical fingerprints of rivers along the Indus-Yalu suture zone in Tibet: implications for timing of arc development and erosion. Geological Society of America Bulletin 129, 570–581. https://doi.org/10.1130/B31587.1.

Carrapa, B., DeCelles, P.G., Reiners, P., Gerhels, G., 2009. Apatite triple dating and white mica $^{40}Ar/^{39}Ar$ thermochronology of syn-tectonic detritus in the Central Andes: a multi-phase tectono-thermal history. Geology 37, 407–410.

Carrapa, B., Orme, D.A., Kapp, P., DeCelles, P.G., Cosca, M., Waldrip, R., 2014. Rapid miocene burial and exhumation of the Indus-Yarlung suture zone in Tibet. Geology 42, 443–446. https://doi.org/10.1130/G35350.1.

Cina, S.E., Yin, A., Grove, M., Dubey, C.S., Shukla, D.P., Lovera, O.M., Kelty, T.K., Gehrels, G.E., Foster, D.A., 2009. Gangdese arc detritus within the eastern Himalayan Neogene foreland basin: implications for the Neogene evolution of the Yalung–Brahmaputra River system. Earth and Planetary Science Letters 285, 150–162. https://doi.org/10.1016/j.epsl.2009.06.005.

Clift, P.D., Hodges, K.V., Heslop, D., Hannigan, R., Van Long, H., Calves, G., 2008. Correlation of Himalayan exhumation rates and Asian monsoon intensity. Nature Geoscience 1, 875–880. https://doi.org/10.1038/ngeo351.

Coogan, J.C., 1992. Structural evolution of piggyback basins in the Wyoming-Idaho-Utah thrust belt. In: Link, P.K., Kentz, M.A., Platt, L.B. (Eds.), Regional Geology of Eastern Idaho and Western Wyoming, 179. Geological Society of America Memoir, pp. 55–81.

Copeland, P., Harrison, T.M., Kidd, W.S.F., Xu, R., Zhang, Y., 1987. Rapid early Miocene acceleration of uplift in the Gangdese Belt, Xizang (southern Tibet), and its bearing on accommodation mechanisms of the India-Asia collision. Earth and Planetary Science Letters 86, 240–252. https://doi.org/10.1016/0012-821X(87)90224-X.

Dai, J., Wang, C., Hourigan, J., Li, Z., Zhuang, G., 2013. Exhumation history of the Gangdese Batholith, Southern Tibetan Plateau: evidence from apatite and zircon (U-Th)/He thermochronology. Journal of Geology 121, 155–172. https://doi.org/10.1086/669250.

DeCelles, P.G., 1994. Late Cretaceous-Paleocene synorogenic sedimentation and kinematic history of the Sevier thrust belt, northeast Utah and southwest Wyoming. Geological Society of America Bulletin 106, 32–56.

DeCelles, P.G., Giles, K.A., 1996. Foreland basin systems. Basin Research 8, 105–123.

DeCelles, P.G., Kapp, P., Quade, J., Gehrels, G.E., 2011. Oligocene-Miocene Kailas basin, southwestern Tibet: record of postcollisional upper-plate extension in the Indus-Yarlung suture zone. Geological Society of America Bulletin 123, 1337–1362. https://doi.org/10.1130/B30258.1.

DeCelles, P.G., Kapp, P., Gehrels, G.E., Ding, L., 2014. Paleocene-Eocene foreland basin evolution in the Himalaya of southern Tibet and Nepal: implications for the age of initial India-Asia collision. Tectonics 33, 824–849.

Dewey, J.F., Bird, J.M., 1970. Mountain belts and the new global tectonics. Journal of Geophysical Research 75, 2625–2647.

Ding, L., Kapp, P., Wan, X., 2005. Paleocene – Eocene record of ophiolite obduction and initial India-Asia collision, south-central Tibet. Tectonics 24, TC3001.

Dumitru, T.A., 1991. Effects of subduction parameters on geothermal gradients in forearcs, with an application to Franciscan subduction in California. Journal of Geophysical Research 96 (1), 621–641.

Dürr, S.B., 1996. Provenance of Xigaze fore-arc basin clastic rocks (Cretaceous, south Tibet). Geological Society of America Bulletin 108, 669–684.

Einsele, G., Liu, B., Dürr, S., Frisch, W., Liu, G., Luterbacher, H.P., Ratschbache, L., Ricken, W., Wendt, J., Wetzel, A., Yu, G., Zheng, H., 1994. The Xigaze forearc basin: evolution and facies architecture (Cretaceous, Tibet). Sedimentary Geology 90, 1–32.

Farley, K.A., 2002. (U-Th)/He dating: techniques, calibrations, and applications. In: Porcelli, D., Ballentine, C.J., Wieler, R. (Eds.), Reviews in Mineralogy and Geochemistry: Noble Gases in Geochemistry and Cosmochemistry, 47. Mineralogical Society of America, Washington, DC, pp. 819–844.

Farley, K.A., Shuster, D.L., Ketcham, R.A., 2011. U and Th zonation in apatite observed by laser ablation ICPMS an implications for the (U–Th)/He system. Geochimica et Cosmochimica Acta 75, 4194–4215.

Fitzgerald, P.G., Stump, E., Redfield, T.F., 1993. Late Cenozoic uplift of Denali and its relation to relative plate motion and fault morphology. Science 259, 497–499.

Flowers, R.M., Ketcham, R.A., Shuster, D.L., Farley, K.A., 2009. Apatite (U-Th)/He thermochronometry using a radiation damage accumulation and annealing model. Geochimica et Cosmochimica Acta 73 (8), 2347–2365.

Fosdick, J.C., Grove, M., Graham, S.A., Hourigan, J.K., Lovera, O., Romans, B.W., 2014. Detrital thermochronologic record of foreland burial heating, sedimentary provenance, and orogenesis in Patagonia. Basin Research 27 (4), 546–572. https://doi.org/10.1111/bre.12088.

Gallagher, K., 2012. Transdimensional inverse thermal history modeling for quantitative thermochronology. Journal of Geophysical Research: Solid Earth 117, B2.

Gansser, A., 1980. The significance of the Himalayan suture zone. Tectonophysics 62, 37–52.

Garzanti, E., Baud, A., Mascle, G., 1987. Sedimentary record of the northward flight of India and its collision with Eurasia (Ladakh Himalaya, India). Geodinamica Acta 1, 297–312.

Gautheron, C., Tassan-Got, L., Barbarand, J., Pagel, M., 2009. Effect of alpha-damage an- nealing on apatite (U–Th)/He thermochronology. Chemical Geology 266, 157–170. https://doi.org/10.1016/j.chemgeo.2009.06.001.

Gautheron, C., Tassan-Got, L., Ketcham, R.A., Dobson, K.J., 2012. Accounting for long alpha- particle stopping distances in (U–Th–Sm)/He geochronology: 3D modeling of diffusion, zoning, implantation, and abrasion. Geochimica et Cosmochimica Acta 96, 44–56. https://doi.org/10.1016/j.gca.2012.08.016.

Girardeau, J., Marcoux, J., Zao, Y., 1984. Lithologic and tectonic environment of the Xigaze ophiolite (Yarlung Zangbo suture zone, Southern Tibet, China), and kinematics of its emplacement. Eclogae Geologicae Helvetiae 77, 153–170.

Guenthner, W.R., Reiners, P.W., Ketcham, R.A., Nasdala, L., Giester, G., 2013. Helium diffusion in natural zircon: radiation damage anisotropy, and the interpretation of zircon (U-Th)/He thermochronology. American Journal of Science 313, 145–198. https://doi.org/10.2475/03.2013.01.

Hager, C., Stockli, D., Dewane, T., Gehrels, G., and Ding, L., Anatomy and HagerHagercrustal evolution of the central Lhasa terrane (S-Tibet) revealed by investigations in the Xainza rift, paper presented in EGU General Assembly Conference Abstracts 11, 2009, 11346, (April 19–24), Vienna.

Harrison, T.M., Yin, A., Grove, M., Lovera, O.M., Ryerson, F.J., Zhou, X., 2000. The Zedong Window: a record of superposed tertiary convergence in southeastern Tibet. Journal of Geophysical Research 105, 19211–19230. https://doi.org/10.1029/2000JB900078.

He, S., Kapp, P., DeCelles, P.G., Gehrels, G.E., Heizler, M., 2007. Cretaceous-tertiary geology of the Gangdese arc in the Linzhou area, southern Tibet. Tectonophysics 433, 15–37.

Heim, A., Gansser, A., 1939. Central Himalaya: Geological Observations of the Swiss Expedition 1936. Hindustan Publishing Corporation, Hindustan, Delhi, 245 pp.

Hodges, K.V., Bowring, S., Davidek, K., Hawkins, D., Krol, M., 1998. Evidence for rapid displacement on Himalayan normal faults and the importance of tectonic denudation in the evolution of mountain ranges. Geology 26, 483–486.

Hourigan, J.K., Reiners, P.W., Brandon, M.T., 2005. U-Th zonation-dependent alpha-ejection in (U-Th)/He chronometry. Geochimica et Cosmochimica Acta 69 (13), 3349–3365.

Hu, H., Sinclair, H.D., Wang, J., Jiang, H., Wu, F., 2012. Late Cretaceous-Paleogene stratigraphic and basin evolution in the Zhepure Mountain of southern Tibet: implications for the timing of India-Asia initial collision. Basin Research 24, 520–543.

Hu, X., Wang, J., BouDagher-Fadel, M., Garzanti, E., An, W., 2015. New insights into the timing of the India-Asia collision from the Paleogene Quxia and Jialazi formations of the Xigaze forearc basin, South Tibet. Gondwana Research 32, 76–92.

Hu, X., Garzanti, E., Wang, J., Huang, W., An, W., Webb, A., 2016. The timing of India-Asia collision onset—facts, theories, controversies. Earth-Science Reviews 160, 264–299. https://doi.org/10.1016/j.earscirev.2016.07.014.

Huang, W., van Hinsbergen, D.J.J., Maffione, M., Orme, D.A., Dupont-Nivet, G., Guilmette, C., Ding, L., Guo, Z., Kapp, P., 2015. The Lower Cretaceous Xigaze ophiolites formed in the Gangdese forearc: evidence from paleomagnetism, sediment provenance, and stratigraphy. Earth and Planetary Science Letters 415, 142–153. https://doi.org/10.1016/j.epsl.2015.01.032.

Johnstone, S., Hourigan, J., Gallagher, C., 2013. LA-ICP-MS depth profile analysis of apatite: protocol and implications for (U-Th)/He thermochronometry. Geochimica et Cosmochimica Acta 109, 143–161.

Kapp, P., Yin, A., Harrison, T.M., Ding, L., 2005. Cretaceous-tertiary shortening, basin development, and volcanism in central Tibet. Geological Society of America Bulletin 117, 865–878.

Kapp, P., Taylor, M., Stockli, D., Ding, L., 2008. Development of active low-angle normal fault systems during orogenic collapse: insight from Tibet. Geology 36 (1), 7–10. https://doi.org/10.1130/G24054A.1.

Ketcham, R.A., 2005. Forward and inverse modeling of low-temperature thermochronometry data. Reviews in Mineralogy and Geochemistry 58, 275–314.

Ketcham, R.A., Gautheron, C., Tassan-Got, L., 2011. Accounting for long alpha-particle stopping distances in (U–Th–Sm)/He geochronology: refinement of the baseline case. Geochimica et Cosmochimica Acta 75, 7779–7791. https://doi.org/10.1016/j.gca.2011.10.011.

Lang, K.A., Huntington, K.W., 2014. Antecedence of Yarlung-Siang-Brahmaputra river, eastern Himalaya. Earth and Planetary Science Letters 370, 145–158. https://doi.org/10.1016/j.epsl.2014.04.026.

Lang, K.A., Huntington, K.W., Burmester, R.F., Housen, B.A., 2016. Rapid exhumation of the eastern Himalayan syntaxis since the Late Miocene. Geological Society of America Bulletin 128. https://doi.org/10.1130/B31419.1.

Laskowski, A.K., Kapp, P., Ding, L., Campbell, C., Liu, X., 2017. Tectonic evolution of the Yarlung Suture zone, Lopu range region, Southern Tibet. Tectonics 36, 108–136. https://doi.org/10.1002/2016TC004334.

Leary, R., Orme, D.A., Laskowski, A.K., DeCelles, P.G., Kapp, P., Carrapa, B., Dettinger, M., 2016. Along-strike diachroneity in the deposition of the Kailas Formation in central southern Tibet: implications for Indian slab rollback. Geosphere 12 (4), 1–26. https://doi.org/10.1130/GES01325.1.

Lee, H.-Y., Ching, S.-L., Lo, C.-H., Ji, J., Lee, T.-Y., Qian, Q., Zhang, Q., 2009. Eocene Nepthethyan slab breakoff in southern Tibet inferred from the Linzizong volcanic record. Tectonophysics 477, 20–35.

Li, G., Kohn, B., Sandiford, M., Xu, Z., Tian, Y., Seiler, C., 2015. Synorogenic morphotectonic evolution of the Gangdese batholith, South Tibet: insights from low-temperature thermochronology. Geochemistry, Geophysics, Geosystems 17, 101–112.

Li, G., Kohn, B., Sandiford, M., Xu, Z., 2017. India-Asia convergence: insights from burial and exhumation of the Xigaze fore-arc basin, south Tibet. Journal of Geophysical Research Solid Earth 122, 3430–3449. https://doi.org/10.1002/2017JB014080.

Maluski, H., Proust, F., Xia, X.C., 1982. ^{39}Ar-^{40}Ar dating of the trans-Himalayan calc-alkaline magmatism of southern Tibet. Nature 298, 152–154.

McDowell, F.W., McIntosh, W.C., Farley, K.A., 2005. A precise ^{40}Ar-^{39}Ar reference age for the Durango apatite (U-Th)/He and fission-track dating standard. Chemical Geology 214, 249–263.

Metcalf, K., Kapp, P., 2017. The Yarlung suture Mélange, Lopu Range, southern Tibet: provenance of sandstone blocks and transition from oceanic subduction to continental collision. Gondwana Research 48, 15–33.

Murphy, M.A., Copeland, P., 2005. Transtensional deformation in the central Himalaya and its role in accommodating growth of the Himalayan orogen. Tectonics 24, TC4012. https://doi.org/10.1029/2004TC001659.

Murphy, M.A., Harrison, T.M., 1999. The relationship between leucogranites and the South Tibetan detachment system, Rongbuk Valley, southern Tibet. Geology 27, 831–834.

Murphy, M.A., Yin, A., 2003. Sequence of thrusting in the Tethyan fold-thrust belt and Indus-Yalu suture zone, southwest Tibet. Geological Society of America Bulletin 115, 21–34.

Murray, K.E., Orme, D.A., Reiners, P.W., 2014. Effects of U-Th-rich grain boundary phases on apatite helium ages. Chemical Geology 390, 135–151.

Najman, Y., Appel, E., Boudagher-Fadel, M., Brown, P., Carter, A., Garzanti, E., Godin, L., Han, J., Oliver, G., Parrish, R., Vezzoli, G., 2010. Timing of India-Asia collision: Geological biostratigraphic, and paleomagnetic constraints. Journal of Geophysical Research 115, B12416. https://doi.org/10.1029/2010JB007673.

Orme, D.A., Laskowski, A.K., 2016. Basin analysis of the Albian-Santonian Xigaze forearc, Lazi region, south-central Tibet. Journal of Sedimentary Research 86, 1–20. https://doi.org/10.2110/jsr.2016.59.

Orme, D.A., Carrapa, B., Kapp, P., 2014. Sedimentology, provenance and geochronology of the upper Cretaceous–lower Eocene western Xigaze forearc basin, southern Tibet. Basin Research. https://doi.org/10.1111/bre.12080.

Orme, D.A., Reiners, P.W., Hourigan, J.K., Carrapa, B., 2015. Effects of inherited cores and magmatic overgrowths on zircon (U-Th)/He ages and age-eU trends from Greater Himalayan sequence rocks, Mt. Everest region, Tibet. Geochemistry, Geophysics, Geosystems 16. https://doi.org/10.1002/2015GC005818.

Pan, G., Ding, J., Yao, D., Wang, L., 2004. Geological Map of the Qinghai-Xizang (Tibet) Plateau and Adjacent Areas. Chengdu Cartographic Publishing House, Chengdu.

Quade, J., Cerling, T.E., Bowman, J.R., 1989. Development of Asian monsoon revealed by marked eco- logical shift during the latest Miocene in northern Pakistan. Nature 342, 163–166.

Quidelleur, X., Grove, M., Lovera, O.M., Harrison, T.M., Yin, A., Ryerson, F.J., 1997. The thermal evolution and slip history of the Renbu Zedong thrust, southeastern Tibet. Journal of Geophysical Research 102, 2659–2679. https://doi.org/10.1029/96JB02483.

Reiners, P.W., 2005. Zircon (U–Th)/He thermochronometry. In: Reiners, P.W., Ehlers, T.A. (Eds.), Low Temperature Thermochronology: Techniques, Interpretations and Applications. Reviews in Mineralogy and Geochemistry, 58, pp. 151–179.

Reiners, P.W., Farley, K.A., 2001. Influence of crystal size on apatite (U-Th)/He thermochronology: an example from the Bighorn Mountains, Wyoming. Earth and Planetary Science Letters 188 (3–4), 413–420.

Reiners, P.W., Farley, K.A., Hickes, H.J., 2002. He diffusion and (U-Th)/He thermochronometry of zircon: initial results from Fish Canyon Tuff and Gold Butte, Nevada. Tectonophysics 349, 297–308.

Reiners, P.W., Spell, T.L., Nicolescu, S., Zanetti, K.A., 2004. Zircon (U-Th)/He thermochronometry: He diffusion and comparisons with ^{40}Ar/^{39}Ar dating. Geochimica et Cosmochimica Acta 68 (8), 1857–1887.

Rhal, J.M., Ehlers, T.A., van der Pluijm, B.A., 2007. Quantifying transient erosion of orogens with detrital thermochronology from syntectonic basin deposits. Earth and Planetary Science Letters 256, 147–161.

Ricci Lucchi, F., 1986. The Oligocene to recent foreland basins of the northern Apennines. In: Allen, P.A., Homewood, P. (Eds.), Foreland Basins, 8. Special Publication International Association of Sedimentology, pp. 105–139.

Robinson, R.A.J., Brezina, C.A., Parrish, R.R., Horstwood, M.S.A., Oo, N.W., Bird, M.I., Thein, M., Walters, A.S., Oliver, G.J.H., Zaw, K., 2013. Large rivers and orogens: the evolution of the Yarlung Tsangpo–Irrawaddy system and the eastern Himalayan syntaxis. Gondwana Research 26, 112–121.

Sanyal, P., Sarkar, A., Bhattacharya, S.K., Kumar, R., Ghosh, S.K., Agrawal, S., 2010. Intensification of monsoon, microclimate and asynchronous C4 appearance: isotopic evidence from the Indian Siwalik sediments. Palaeogeography, Palaeoclimatology, Palaeoecology 296, 165–173.

Schärer, U., Xu, R.H., Allègre, C.J., 1984. U-Pb geochronology of Gangdese (Transhimalaya) plutonism in the Lhasa-Xigaze region, Tibet. Earth and Planetary Science Letters 69, 311–320.

Schmitz, M.D., Bowring, S.A., 2001. U-Pb zircon and titanite systematics of the Fish Canyon Tuff: an assessment of high precision U-Pb geochronology and its application to young volcanic rocks. Geochimica et Cosmochimica Acta 65, 2571–2587.

Shuster, D.L., Flowers, R.M., Farley, K.A., 2006. The influence of natural radiation damage on helium diffusion kinetics in apatite. Earth and Planetary Science Letters 249, 148–161.

Sobel, E.R., Dumitru, T.A., 1997. Thrusting and exhumation around the margins of the western Tarim basin during the India-Asia collision. Journal of Geophysical Research 102 (3), 5043–5063.

Spiegel, C., Kohn, B., Belton, D., Berner, Z., Gleadow, A., 2009. Apatite (U–Th–Sm)/He thermochronology of rapidly cooled samples: the effect of He implantation. Earth and Planetary Science Letters 285, 105–114.

Styron, R., Taylor, M., Sundell, K., 2015. Accelerated extension of Tibet linked to the northward underthrusting of Indian crust. Nature Geoscience 8 (2), 131–134.

Sundell, K.E., Taylor, M.H., Styron, R.H., Stockli, D.F., Kapp, P., Hager, C., Liu, D., Ding, L., 2013. Evidence for constriction and Pliocene acceleration of east-west extension in the North Lunggar rift region of west central Tibet. Tectonics 32, 1–26. https://doi.org/10.1002/tect.20086.

Taylor, M., Yin, A., 2009. Active structures of the Himalayan-Tibetan orogen and their relationships to earthquake distribution, contemporary strain field, and Cenozoic volcanism. Geosphere 5 (3), 199–214.

Tremblay, M.M., Fox, M., Schmidt, J.L., Tripathy-Lang, A., Wielicki, M.M., Harrison, T.M., Zeitler, P.K., Shuster, D.L., 2015. Erosion in southern Tibet shut down at 10 Ma due to enhanced rock uplift within the Himalaya. Proceedings of the National Academy of Sciences of the United States of America 112 (39), 12030–12035.

Vermeesch, P., Tian, Y., 2014. Thermal history modeling: HeFTy vs. QTQt. Earth-Science Reviewers 139, 279–290.

Wagner, G.A., Reimer, G.M., 1972. Fission track tectonics: the tectonic interpretation of fission track apatite ages. Earth and Planetary Science Letters 14, 263–268.

Wang, C.S., Li, X.H., Hu, X.M., Jansa, L.F., 2002. Latest marine horizon North of Qomolangma (Mt Everest): implications for closure of Tethys seaway and collision tectonics. Terra Nova 14, 114–120.

Wang, J., Hu, X., Jansa, L., Huang, Z., 2011. Provenance of the Upper Cretaceous–Eocene deep-water sandstones in Sangdanlin, southern Tibet: constraints on the timing of initial India-Asia collision. Journal of Geology 119, 293–309.

Wang, C., Li, X., Liu, Z., Li, Y., Jansa, Y., Dai, J., Wei, Y., 2012. Revision of the Cretaceous-Paleogene stratigraphic framework, facies architecture and

provenance of the Xigaze forearc basin along the Yarlung Zangbo suture zone. Gondwana Research 22 (2), 415–433. https://doi.org/10.1016/.
Wang, J.-G., Hu, X., Garzanti, E., An, W., Liu, X.-C., 2017. The birth of the Xigaze forearc basin in southern Tibet. Earth and Planetary Science Letters 465, 48–47.
Wu, F.-Y., Ji, W.-Q., Liu, C.-Z., Chung, S.-L., 2010. Detrital zircon U-Pb and Hf isotopic data from the Xigaze fore-arc basin: constraints on Transhimalayan magmatic evolution in southern Tibet. Chemical Geology 271, 13–25.
Xiong, Q., Griffin, W.L., Zheng, J.-P., Pearson, N.J., O'Reilly, S.Y., 2017. Two-layered oceanic lithospheric mantle in a Tibetan ophiolite produced by episodic subduction of Tethyan slabs. Geochemistry, Geophysics, Geosystems 18, 1189–1213.
Yin, A., Harrison, T.M., 2000. Geologic evolution of the Himalayan-Tibetan orogen. Annual Review of Earth and Planetary Sciences 28, 211–280.
Yin, A., Harrison, T.M., Ryerson, F.J., Chen, W., Kidd, W.S.F., Copeland, P., 1994. Tertiary structural evolution of the Gangdese thrust system, southeastern Tibet. Journal of Geophysical Research 99, 18175–18201.
Yin, A., Harrison, T.M., Murphy, M., Grove, M., Nie, S., Ryerson, F., Feng, W.X., Le, C.Z., 1999. Tertiary deformation history of southeastern and southwestern Tibet during the Indo-Asian collision. Geological Society of America Bulletin 111, 1644–1664.
Zeitler, P., Herczeg, A., McDougall, I., 1987. U–Th–He dating of apatite: a potential thermochronometer. Geochimica et Cosmochimica Acta 51, 2865–2868.
Zhang, R., Murphy, M.A., Lapen, T.J., Sanchez, V., Heizler, M., 2011. Late Eocene crustal thickening followed by Early-Late Oligocene extension along the India-Asia suture zone: evidence for cyclicity in the Himalayan orogen. Geosphere 7 (5), 1249–1268.
Zhang, Q., Willems, H., Ding, L., Grafe, K.-U., Appel, E., 2012. Initial India-Asia continental collision and foreland basin evolution in the Tethyan Himalaya of Tibet: Evidence from stratigraphy and paleontology. Journal of Geology 120, 175–189.
Zhu, B., Kidd, W.S.F., Rowley, D.B., Currie, B.S., Shafique, N., 2005. Age of initiation of the India-Asia collision in the east-central Himalaya. Journal of Geology 113, 265–285.

Please cite this article in press as: Orme, D.A., Burial and exhumation history of the Xigaze forearc basin, Yarlung suture zone, Tibet, Geoscience Frontiers (2017), https://doi.org/10.1016/j.gsf.2017.11.011